ORNL/TM--8845

DE84 002410

Engineering Technology Division

EXPERIMENTAL STRESS ANALYSIS OF FOUR MACHINED 10-IN. NPS PIPING ELBOWS WITH SPECIFIED GEOMETRIC DISTORTIONS

S. E. Moore W. G. Dodge
S. E. Bolt

Date Published - September 1983

Prepared by the
OAK RIDGE NATIONAL LABORATORY
Oak Ridge, Tennessee 37830
operated by
UNION CARBIDE CORPORATION
for the
U.S. DEPARTMENT OF ENERGY
under Contract No. W-7405-eng-26

DISCLAIMER

CONTENTS

NOMENCLATURE

A_n, C_n	Fourier coefficients
$B_1(\phi)$	dimensionless function for elliptical elbows
b, c	in-plane and out-of-plane diameters for elliptical elbows
C_2	in-plane bending-moment primary-plus-secondary stress index for ideal geometry elbows
C_2'	in-plane bending-moment primary-plus-secondary stress index for elliptical elbows
D_m	$(D_o - t)$, mean outside diameter (in.)
D_o	average outside diameter (in.)
D_{max}	maximum outside diameter (in.)
D_{min}	minimum outside diameter (in.)
E	modulus of elasticity, nominally 29.0×10^6 (psi)
e	$[1 - (b/c)^2]^{1/2}$, eccentricity of elliptical elbows
$f(\lambda, \psi)$	moment-loading stress-index reduction factor for elbows also loaded with internal pressure
K_1	peak stress index for internal pressure
M_i	in-plane moment load (in.-lb)
M_o	out-of-plane moment load (in.-lb)
M_t	torsional moment load (in.-lb)
$\bar{M}_o$	out-of-plane moment vector (in.-lb)
$\bar{M}_t$	torsional moment vector (in.-lb)
P	internal pressure (psi)
R	bend radius of elbow, nominally 15 in.
r	$D_m/2$, mean pipe radius of elbow (in.)
t	average wall thickness (in.)
Z	$\pi r^2 t$, approximate section modulus ($in.^3$)
α	longitudinal position angle on elbow (deg)
ϕ	circumferential position angle on elbow starting with $\phi = 0$ at intrados (deg)
ξ	longitudinal position angle relative to α (deg)
λ	$tR/(r^2\sqrt{1 - \nu^2})$, dimensionless elbow bend characteristic
ψ	PR^2/Ert, dimensionless pressure parameter
$\sigma_{\alpha m}$	longitudinal membrane-stress index
$\sigma_{\phi m}$	circumferential membrane-stress index

$\sigma_{\alpha b}$	longitudinal shell-bending stress index
$\sigma_{\phi b}$	circumferential shell-bending stress index
$\sigma_{\alpha i}$	longitudinal inside-surface stress index
$\sigma_{\alpha o}$	longitudinal outside-surface stress index
$\sigma_{\phi i}$	circumferential inside-surface stress index
$\sigma_{\phi o}$	circumferential outside-surface stress index
$\bar{\sigma}_{max}$	maximum principal stress index
$\bar{\sigma}_{min}$	minimum principal stress index
ν	Poisson's ratio, nominally 0.3

FOREWORD

The work reported here was performed at the Oak Ridge National Laboratory (ORNL) in support of the ORNL Piping Program. The experimental work was performed for the U.S. Atomic Energy Commission prior to formation of the U.S. Department of Energy. Analysis of the data and publication of this report was funded by the David W. Taylor Naval Ship Research and Development Center (DTNSRDC), Annapolis, Maryland, under contract No. N 61533-80-GO-00016. L. M. Kaldor, Code 2744, is the DTNSRDC project engineer. S. E. Moore, Engineering Technology Division, ORNL, is the Program Manager.

ACKNOWLEDGMENTS

The authors are indebted to E. H. Guinn and J. P. Rudd for constructing and instrumenting the models and for running the tests under the direction of S. E. Bolt. We are also indebted to T. C. Gwaltney, Engineering Technology Division (ETD), Oak Ridge National Laboratory, and to S. K. Iskander of the Computer Sciences Division for conducting certain analytical studies in addition to those performed by the authors. F. M. O'Hara and Virginia Hamrick provided extensive editorial assistance in preparing the manuscript. Finally, we gratefully acknowledge the assistance of the ETD Word Processing Center for typing the report and the ETD Publications Office for final processing.

EXPERIMENTAL STRESS ANALYSIS OF FOUR MACHINED 10-IN. NPS PIPING ELBOWS WITH SPECIFIED GEOMETRIC DISTORTIONS

S. E. Moore W. G. Dodge
S. E. Bolt

ABSTRACT

Four specially fabricated nominal 10-in. NPS, 90°, long-radius, schedule 40, carbon-steel piping elbows, welded to short lengths of straight pipe, were stress analyzed both experimentally and analytically. One elbow had a circular cross section and a uniform wall thickness, while the other three had either a circular or elliptical cross section with either a uniform or variable wall thickness. The objectives of the tests were primarily to study the influence of out of roundness and wall-thickness variations on the stresses in piping elbows under internal pressure and/or applied moment loadings. Analytical studies were made to isolate the various effects by comparing the experimental data with theoretical baseline solutions. Results of the studies showed that analytical solutions based on no-end-effects (NEE) theory capture the major characteristics of the stress distributions for elbows loaded with pressure and/or in-plane, out-of-plane, or torsional moment loadings. Of the four second-order effects addressed in this study, end effects had the most influence on the stresses, followed in order by out of roundness, wall-thickness variations, and pressure-moment interactions. Of these, the only significant increase in maximum stresses above those predicted by NEE theory was for the case of out of roundness with internal-pressure loading.

1. INTRODUCTION

Specific dimensional tolerances, other than those of the accepted manufacturing standards,[1,2] are not included in the rules of the American Society of Mechanical Engineers (ASME) Boiler and Pressure Vessel Code[3] on the presumption that any significant effects will be accounted for in the design process. Rules are given in the Code* for evaluating the effects

*The term "Code" as used hereinafter refers to the ASME Boiler and Pressure Vessel Code, Sect. III, Div. 1, 1980 edition. References to specific portions of the Code are identified by the Code numbering system (e.g., NB-3600).

of out of roundness of piping products under internal-pressure loads (NB-3683.2), but rules are not given for out of roundness under moment loads or for variations in wall thickness under either internal-pressure or moment loadings.

The study described in this report was conducted primarily to obtain experimental stress analysis data on the effects of out of roundness and variations in wall thickness for piping elbows with internal pressure and/or applied-moment loadings. Two other objectives were to also study the effects of end restraint from the attached piping (end effects) and the effects of internal-pressure-loading and moment-loading interactions.

So that these objectives could be accomplished, four nominal 10-in. NPS, 90°, long-radius, schedule 40, carbon-steel piping elbows were specially manufactured with controlled variations in out of roundness and wall thickness. Short lengths of straight pipe were welded to each end of the elbows to form test models. The test models were then instrumented with strain gages and tested with internal-pressure and in-plane, out-of-plane, and torsional moment loads applied individually and with combined pressure-moment loads. Various theoretical stress analysis solutions for elbows loaded with internal pressure and applied moments were used as comparative standards to isolate the different effects being studied experimentally.

The four test models and their planned dimensional variations are identified in Table 1.1. Figure 1.1 is a schematic of the test model loadings. Model ME-1 was planned to be as geometrically perfect as possible, so that the elastic-response data could be used as the standard baseline for comparing the results from the other models. The effects of out of roundness (initial "ovaling") and variable wall thickness were to be determined by comparing results from models ME-2 and ME-3 with results from ME-1. The fourth model, ME-4, with both initial ovaling and a variable wall thickness, was included to test the assumption of stress superposition for nonlinear changes in geometry. In addition, the experimental results were to be compared with various theoretical solutions to help isolate and identify the effects being studied.

Table 1.1. Machined-elbow test models

Model	Identification	Model parameters
ME-1	Ideal torus	90°, long radius, 10.750-in. nominal OD, uniform wall 0.365 in. thick
ME-2	Ovaled torus	90°, long radius, 10.750-in. nominal OD, uniform wall 0.365 in. thick, flattened 5–8% of the diameter[a]
ME-3	Thinned elbow	90°, long radius, 10.750-in. nominal OD, bore eccentric 0.093 in.,[b] minimum wall 0.272 in., maximum wall 0.458 in.
ME-4	Ovaled and thinned elbow	90°, long radius, 10.750 in. nominal OD, bore eccentricity 0.093 in.,[b] minimum wall 0.272 in., maximum wall 0.458 in., flattened 5–8% of the diameter[a]

[a]An attempt was to be made to form an elliptical cross section with a major-to-minor diameter ratio between 1.05 and 1.08 and with the major axis lying in the plane of the bend.

[b]The eccentricity of the bore was to be away from the center of the bend so that the minimum wall thickness would be along the back of the elbow (extrados).

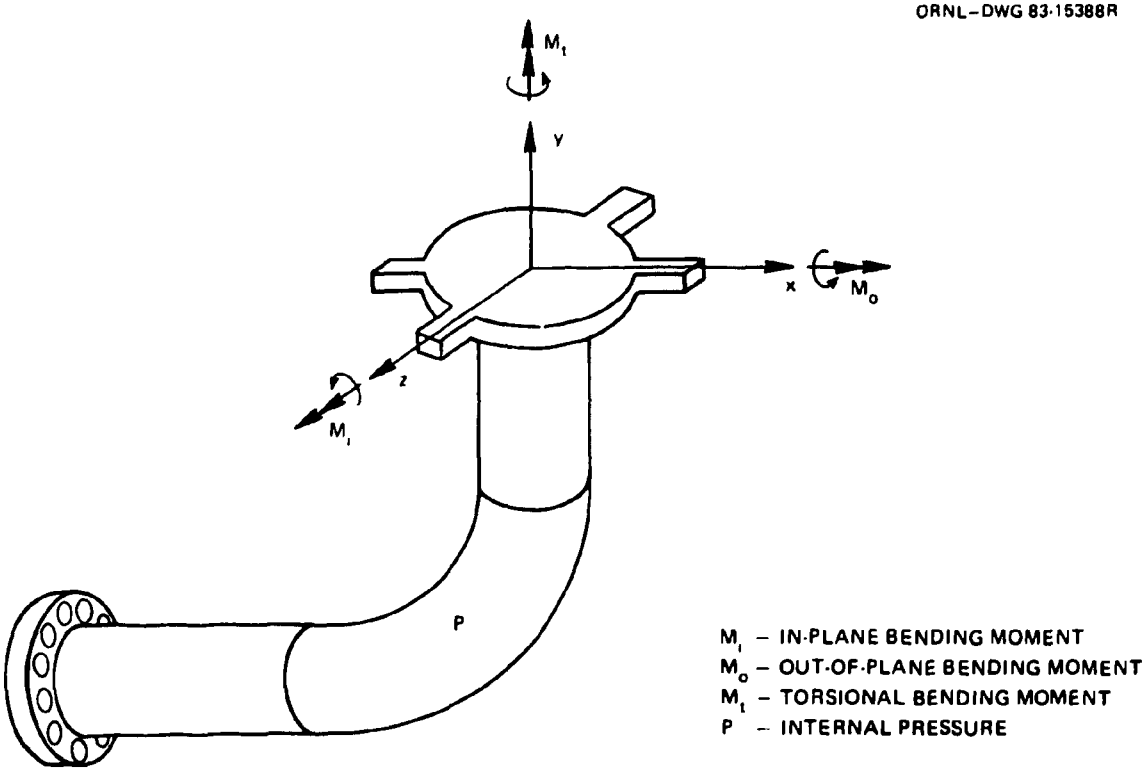

Fig. 1.1. Schematic diagram of test model loadings.

Fabrication and inspection, instrumentation, and the test setup are described in the next chapter. Chapter 3 describes the experimental procedures and reduction of the strain gage data. Experimental results and comparisons with various analytical models are given in Chap. 4. Chapter 5 gives a summary of the important conclusions. Wall-thickness and outside-diameter measurements for each elbow model are listed in Appendix A. The reduced strain gage data and normalized stresses for each model and for each loading are tabulated in Appendix B. These appendixes are on microfiche in the envelope attached to the inside back cover.

2. FABRICATION, INSTRUMENTATION, AND TEST SETUP

2.1 Fabrication and Inspection

Each of the four test models consisted of a specially fabricated 90°, long-radius, nominal 10-in. NPS, schedule 40, carbon-steel, butt-welding elbow, with short lengths of straight pipe welded to the elbows and suitable end closures and loading fixtures. The elbows were made from ASTM A106 grade B carbon-steel seamless tubing with 0.420-in.-thick walls.

Because we intended to study the effects of dimensional variations on the stresses, the elbows were specially fabricated (by Crane Manufacturing Company in St. Louis, Missouri) by a combination of forming and machining operations. The seamless tubing was first heated in a furnace, then forced lengthwise over a 10-in. long-radius forming horn, which produced a pipe bend of uniform wall thickness with short, straight tangent ends. While still hot the bend was pressed in a sizing die and finally given a full-anneal heat treatment. Each model was then machined on the inside surface to the final dimensions using special equipment developed by the manufacturer. The tangent stub ends were left on the elbows so that there would not be a weld joint at the elbow-to-straight-pipe intersection to interfere with planned strain gage sites.

Model ME-1 was machined with a round cross section and a uniform wall thickness to serve as the reference "ideal torus" model. Model ME-2 was machined round with a uniform wall thickness, then laid on its side in a press, and flattened uniformly along its length to form an ovaled cross section with the major axis of the oval in the plane of the bend. Model ME-3, the "thinned" model, was machined with a round inside surface whose axis was displaced toward the extrados, so that the wall thickness varied continuously around the circumference but was constant along its length. Model ME-4 was both thinned and ovaled to combine the major features of models ME-2 and ME-3.

Preliminary inspection at the manufacturer's plant indicated that the dimensions of the elbow were not as well controlled as intended. Therefore, after the elbows were received at Oak Ridge National Laboratory (ORNL), a complete dimensional profile of each elbow was developed. A

rectangular grid, consisting of longitudinal and circumferential lines, was lightly scribed at the outside surface of each elbow. The longitudinal lines, called ϕ lines, were located at 22.5° intervals around the circumference, starting with $\phi = 0°$ at the intrados. The circumferential lines, called stations, were located at 15° intervals along the axis starting with station 4 at one end of the elbow and ending with station 10 at the other end. Stations 1, 2, and 3 were assigned to the pipe stubs for locating strain gages. Figure 2.1 shows the position of the instrumented stations (1 through 10) and ϕ lines for one of the test models in relation to the loading frame.

A complete set of wall thicknesses and outside diameters were measured at every grid point for each elbow. These are listed in Appendix A. No dimensional data were obtained for the pipe stubs. The significant dimensional parameters of each test model are given in Table 2.1. Figures 2.2 and 2.3 show the variation of the wall thicknesses and outside diameters from their mean values, respectively.

Although the dimensions of the elbows deviated somewhat from the specification of Table 1.1, they did exhibit the major features intended. As planned, both ME-1 and ME-3 were essentially perfect toroids with less than 1% out of roundness. Models ME-2 and ME-4 were essentially elliptical toroids with about 5% out of roundness. Models ME-1 and ME-2 were centerline bored so that the wall thickness was essentially uniform around the circumference, but random variations in wall thickness were greater than desired. Models ME-3 and ME-4 were bored off-center as planned, but the eccentricity was considerably less than specified so that the variation in wall thickness around the circumference was less than intended. Both the average wall thickness and random variations in wall thickness were greater than planned for all four models.

After the dimensions of the elbows were determined, 10-in. NPS, schedule 40, carbon-steel pipe stubs were welded to each end of the elbow tangents. To ensure a proper fit at the weld, we flattened one-pipe-diameter lengths of the pipe stubs to match the ovaled elbows (ME-2 and ME-4); one-half-pipe-diameter lengths of the stubs were tapered by grinding to match the thinned models (ME-2 and ME-4). The pipe stubs were between 17 and 19 in. long, which was long enough to ensure die-out of the discontinuity stresses from the loading fixtures.

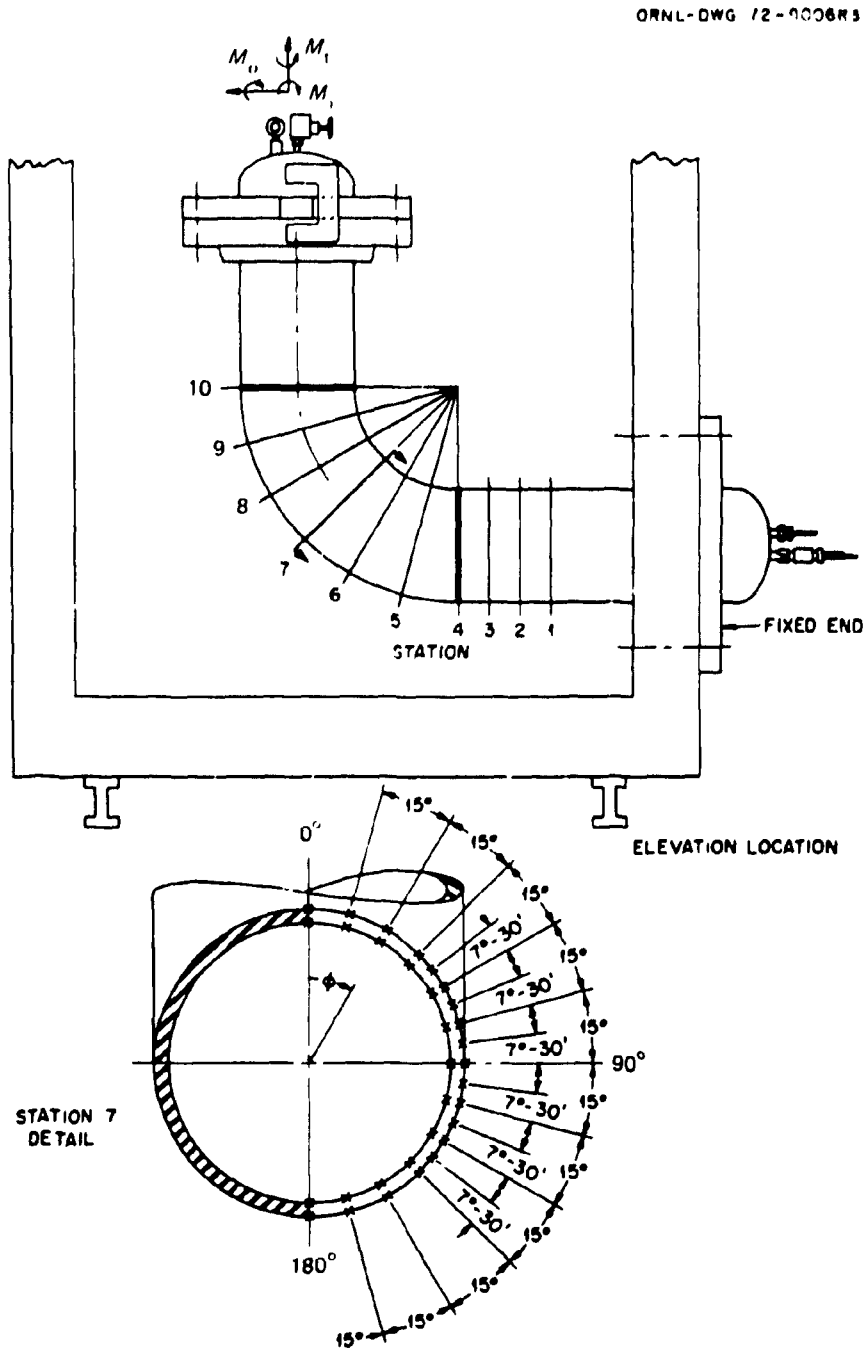

Fig. 2.1. Schematic diagram of instrumented stations and ϕ lines for elbow test models.

Table 2.1. Significant dimensional parameters for elbow test models

Parameter[a]	Elbow model				Pipe[b] stub
	ME-1	ME-2	ME-3	ME-4	
Average wall thickness, t, in.	0.390	0.384	0.370	0.358	0.365
Minimum wall thickness, in.	0.366	0.345	0.279	0.280	
Maximum wall thickness, in.	0.408	0.409	0.414	0.418	
Centerline eccentricity, in.	0.001	0.014	0.038	0.047	
Average outside diameter, D_o, in.	10.716	10.728	10.754	10.734	10.750
Mean radius, r, in.	5.163	5.172	5.192	5.188	5.193
In-plane diameter, b, in.	10.354	10.560	10.356	10.560	
Out-of-plane diameter, c, in.	10.284	9.972	10.408	10.032	
Average ellipticity,[c] aspect ratio	1.006	1.048	0.991	1.041	
Percent flattening[d]	0.67	5.34	0.97	4.71	
Section modulus, $Z = \pi r^2 t$, in.^{3}	32.660	32.270	31.334	30.271	30.917
Bend characteristic, $\lambda = tR/(r^2\sqrt{1-\nu^2})$	0.2300	0.2257	0.2158	0.2091	
Pressure parameter, $\psi/P = R^2/Ert$, 10^{-6}/psi	3.856	3.902	4.038	4.176	

[a] Bend radius R, modulus of elasticity E, and Poisson's ratio ν, were not measured. Their values were assumed to be R = 15.0, E = 29.0 x 10^6, and ν = 0.3.

[b] Nominal dimensions.

[c] Ellipticity is defined as the ratio of the in-plane to out-of-plane diameters of the best-fit ellipse. The shape of all four models deviated from elliptical by less than 1%.

[d] Percent flattening is defined as $(D_{max} - D_{min})/D_o \times 100$.

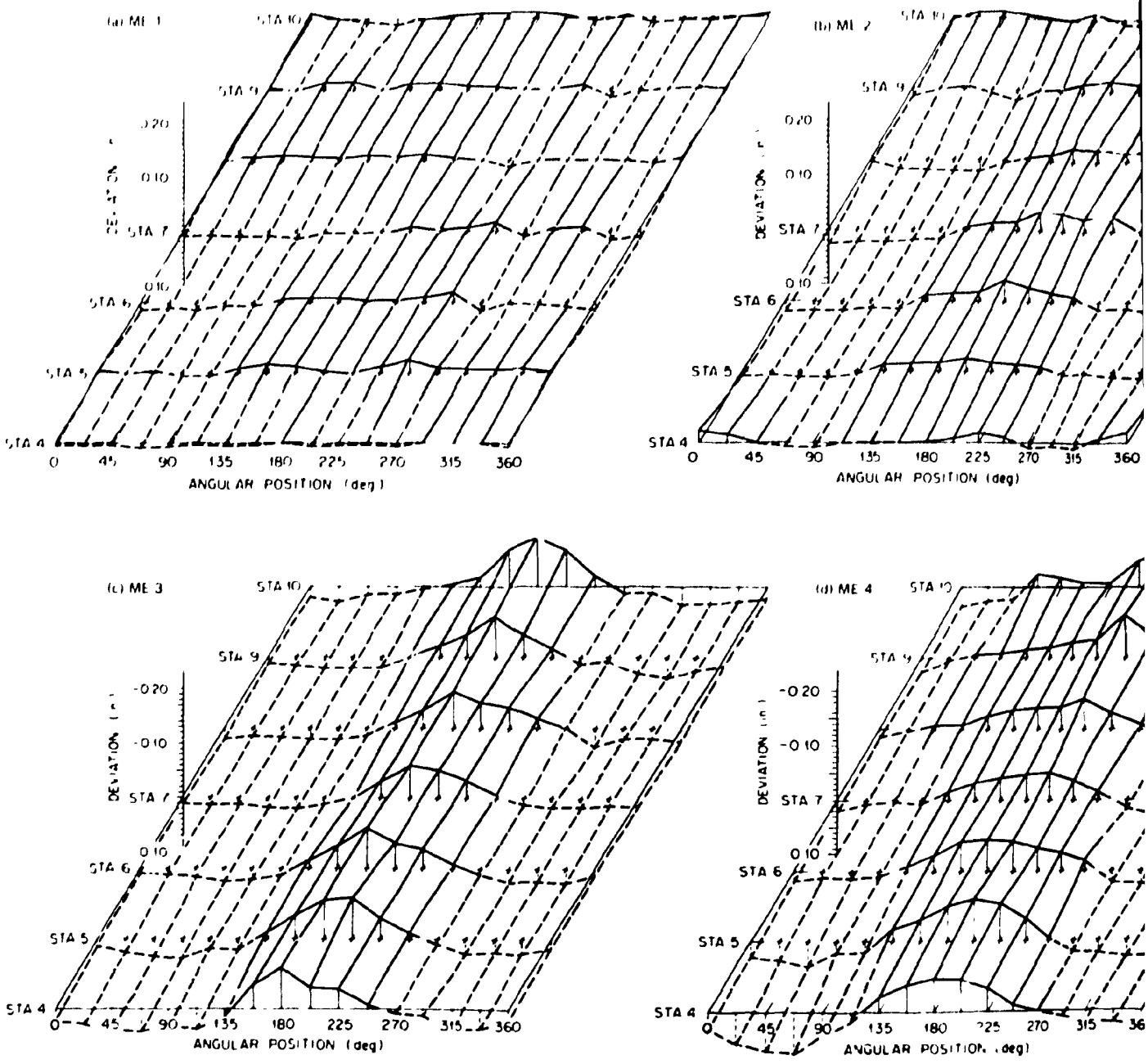

Fig. 2.2. Wall thickness deviations from the mean for each of the four test models.

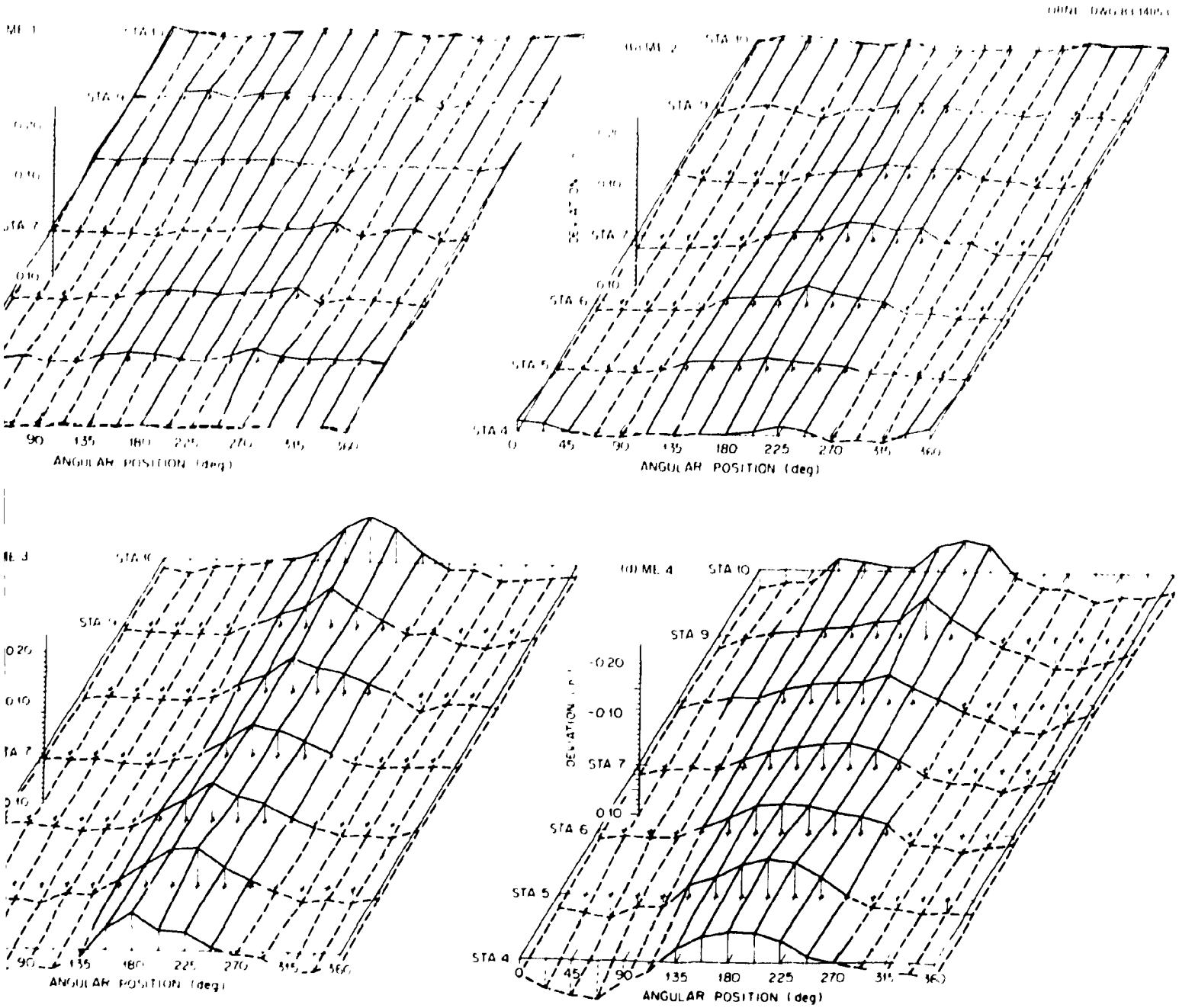

Fig. 2.2. Wall thickness deviations from the mean for each of the four test models.

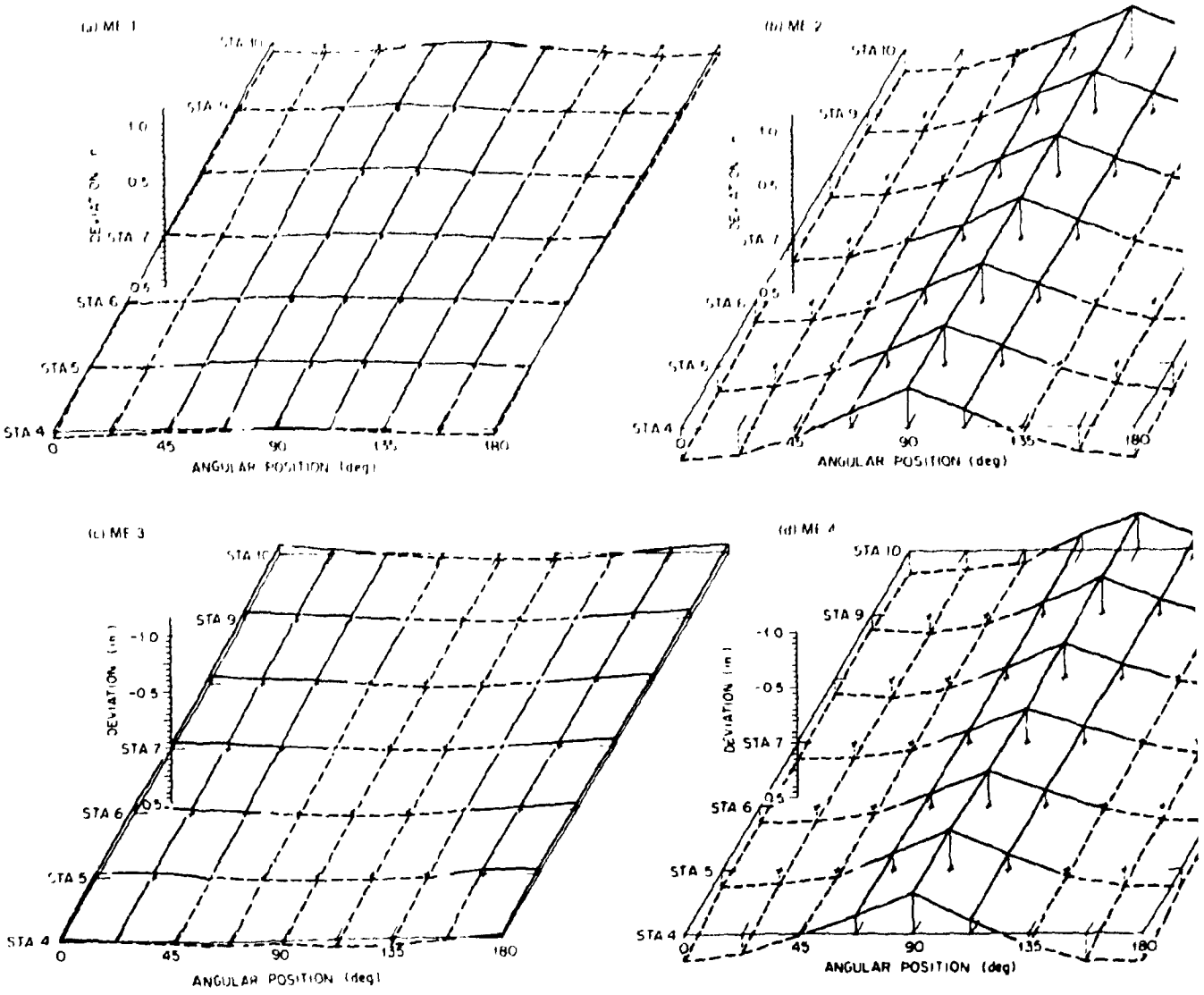

Fig. 2.3. Outside diameter variations from the mean for each of the four test models.

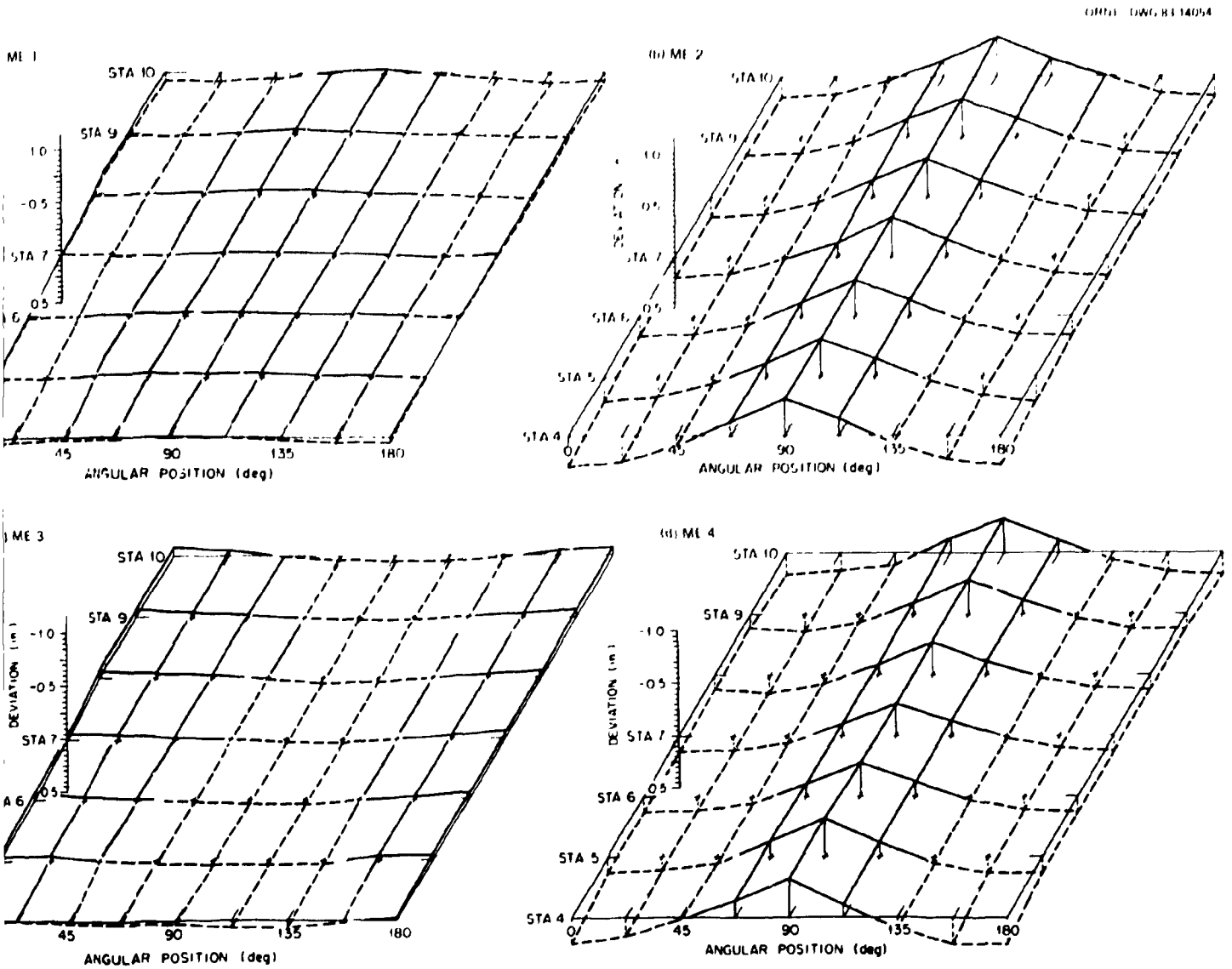

Fig. 2.3. Outside diameter variations from the mean for each of the four test models.

2.2 Instrumentation

Each model was instrumented with approximately 90 three-gage 45° strain rosettes, with the majority placed on the outside surface. The strain gage locations for each model are identified in Figs. 2.4–2.11. The orientation was such that the middle leg (gage 2) was on a circumferential line of the test model. Station 7, which bisects the elbow, was the most heavily instrumented, with 19 rosettes on the outside surface and 13 on the inside surface. The stress distributions at this position correspond most closely with those obtained from analytical models that neglect end effects.

Except for station 7 of ME-1, all of the strain gages were 1/8-in. constantan foil Micro-Measurements type EA-06-125RA-120, option W, 45° rosettes, mounted on a flexible polymide backing and temperature compensated for use on carbon steel. The 13 rosettes mounted at station 7 on the inside surface of ME-1 were 1/16-in. Micro-Measurements, type EA-06-062RB-120, option SE constantan foil gages. A high-performance epoxy-phenolic adhesive (Micro-Measurements M Bond 600) was used to bond the rosettes to the models. The adhesive was cured for 2 h at 300°F under a clamping pressure of 15 psi.

Gages for measuring the strain distributions along the length of the elbows were mounted on the outside surface at stations 1 through 6 over the quadrant between $\phi = 90°$ and 180°. A few gages were also installed on the inside surface at station 1 to determine through-the-wall bending stresses near the middle of the pipe stubs. Other gages were installed to provide symmetry checks.

When the strain gage installation was completed and checked for continuity, the instrumentation lead wires from the inside gages were routed through a packing gland and the model was sealed with end caps welded to the pipe stubs. Class 900 slip-on flanges were then welded to each end of the test model for mounting the model in the loading frame and attaching the cross-beam loading fixture. Dial gages and load cells were installed for measuring model deflections and applied loads. Several of the dial gages can be seen in Fig. 2.12, which shows ME-1 ready for testing.

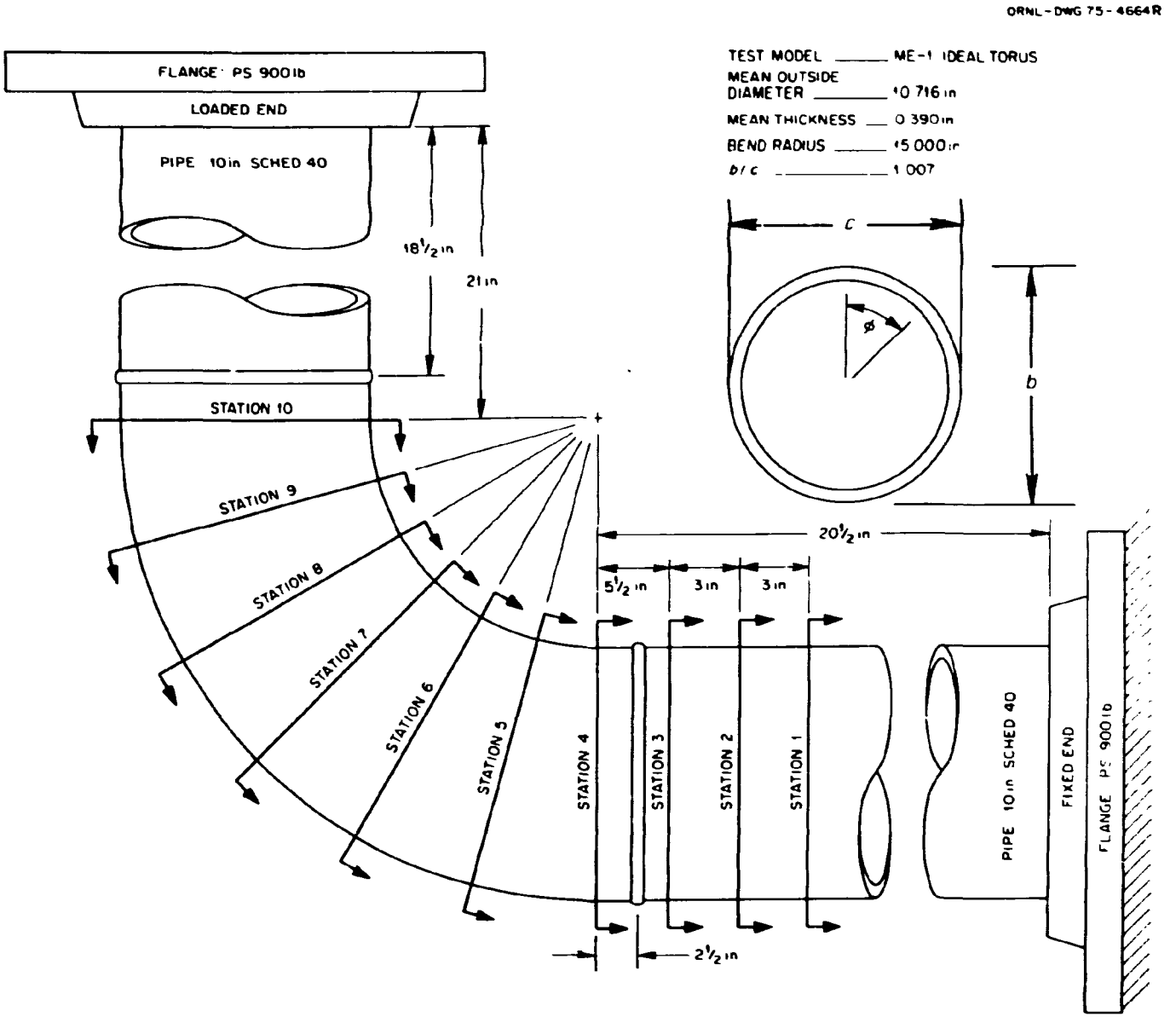

Fig. 2.4. Dimensional data for test model ME-1.

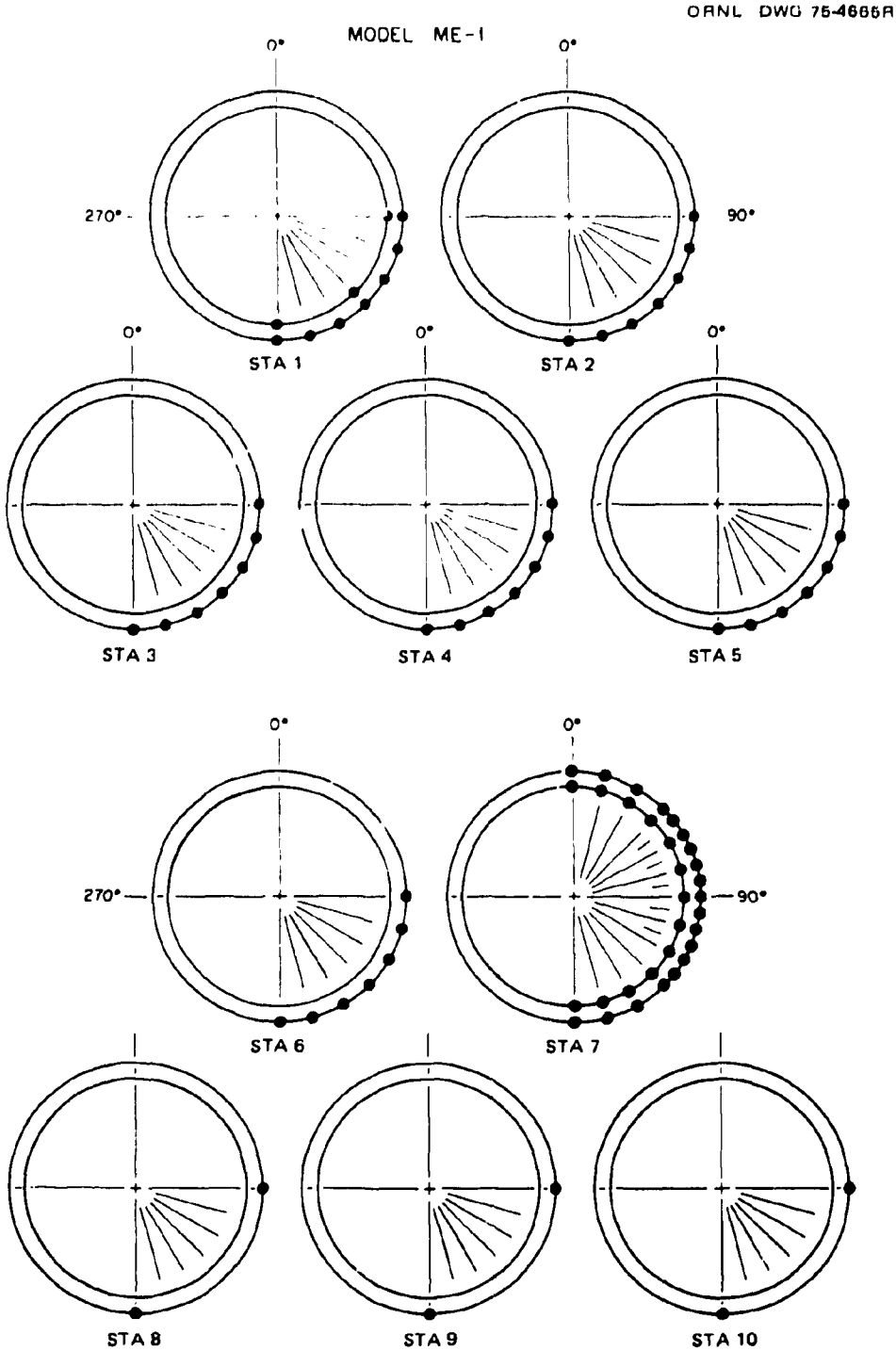

Fig. 2.5. Strain gage locations for test model ME-1.

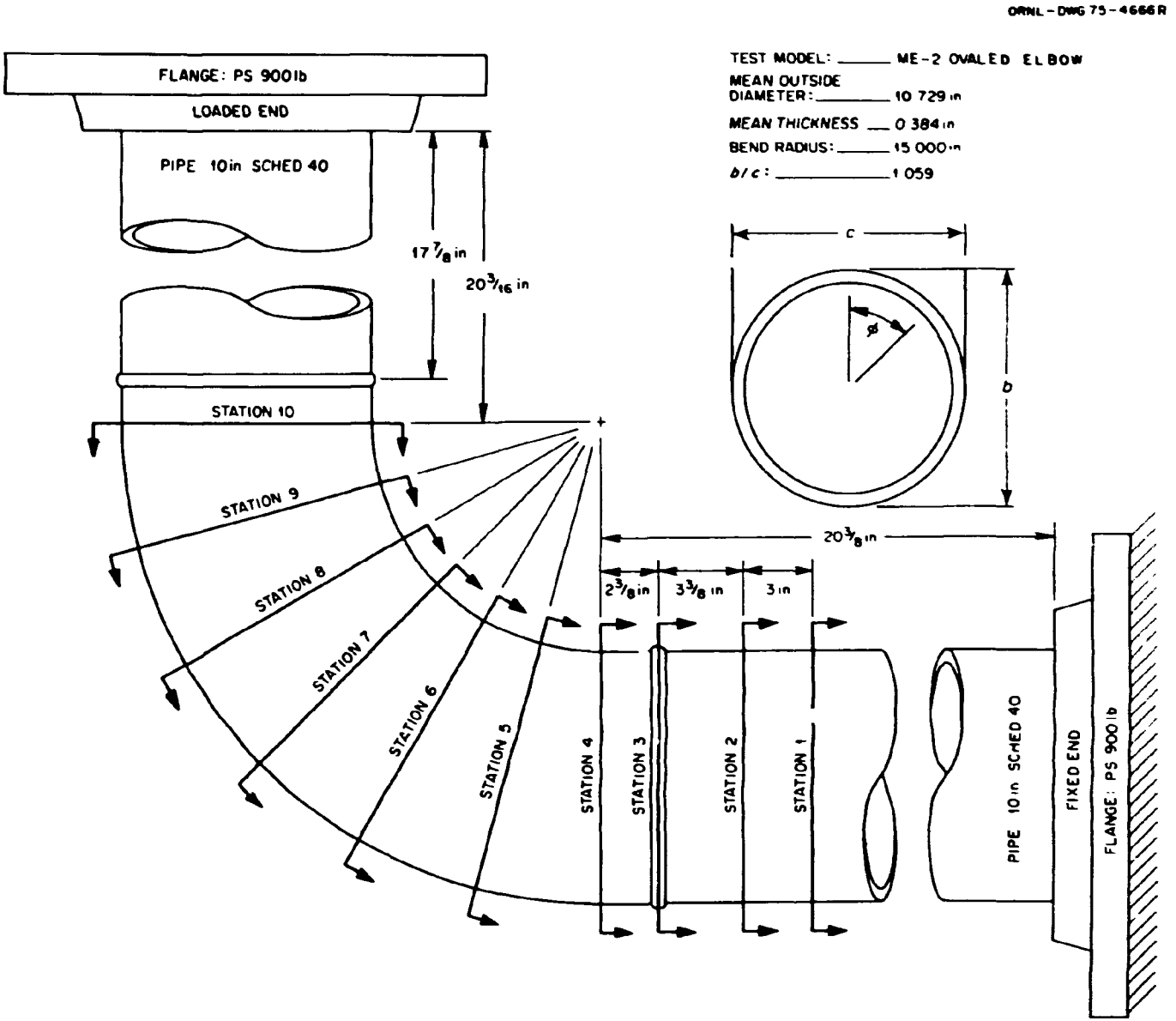

Fig. 2.6. Dimensional data for test model ME-2.

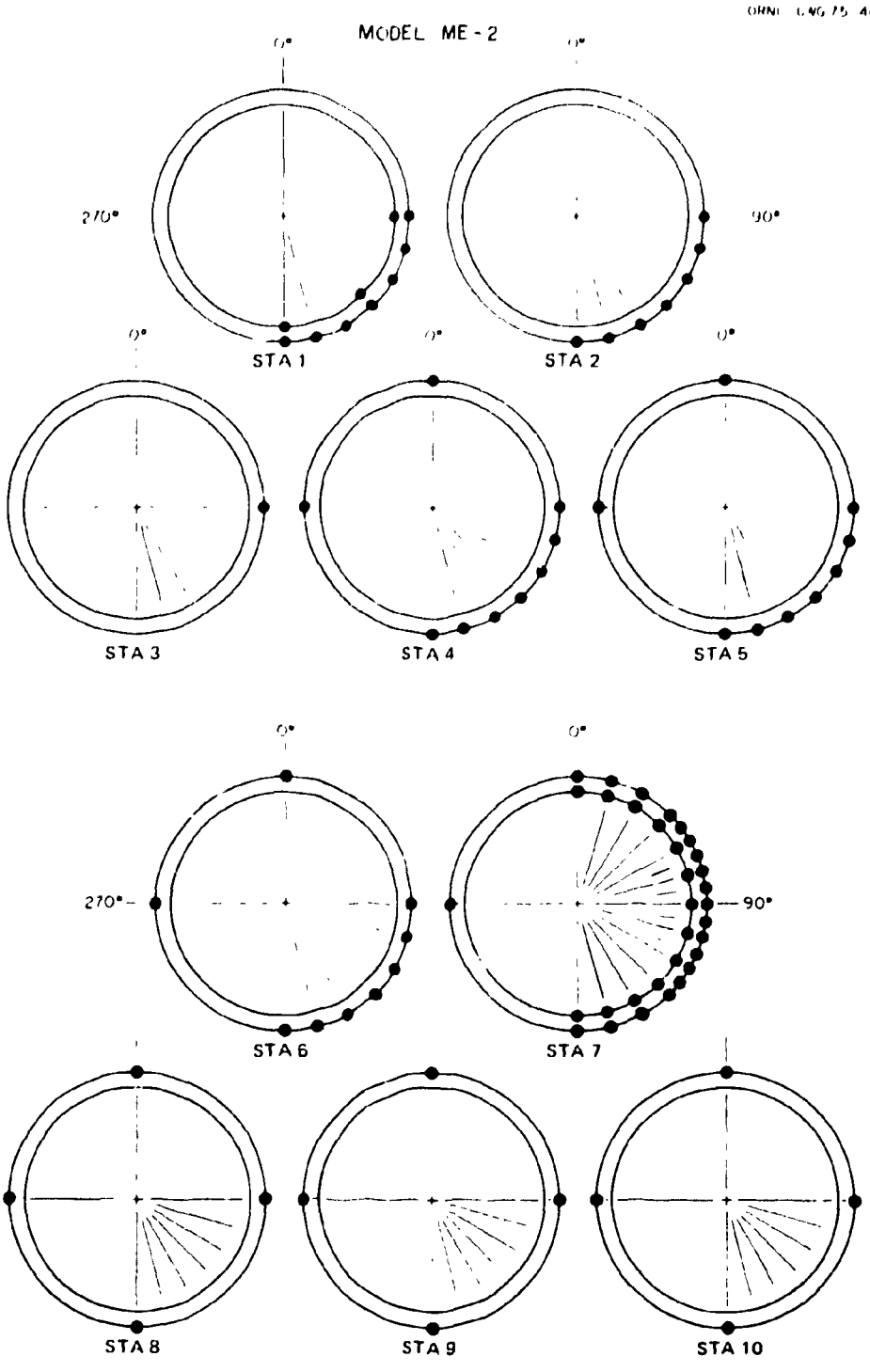

Fig. 2.7. Strain gage locations for test model ME-2.

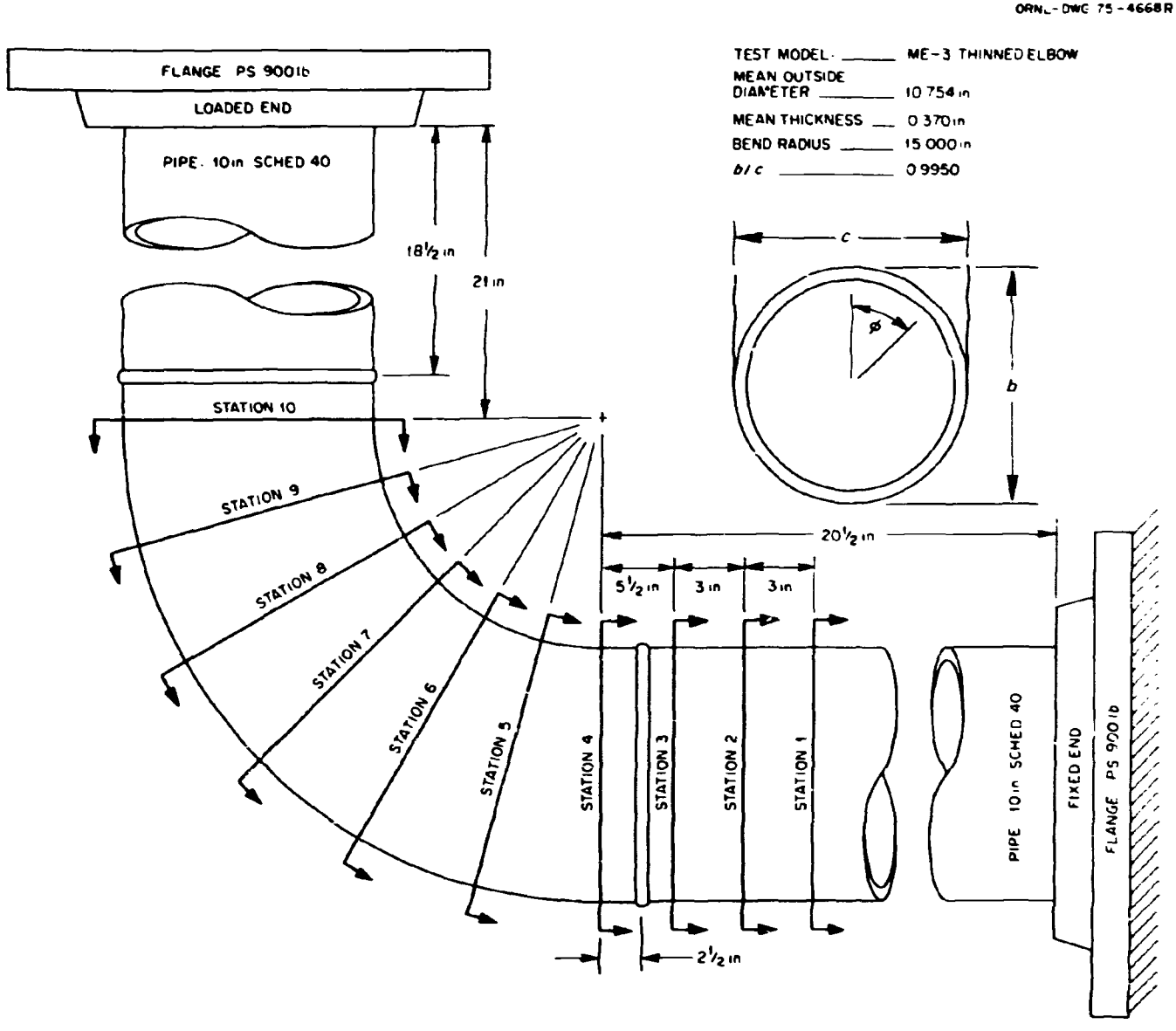

Fig. 2.8. Dimensional data for test model ME-3.

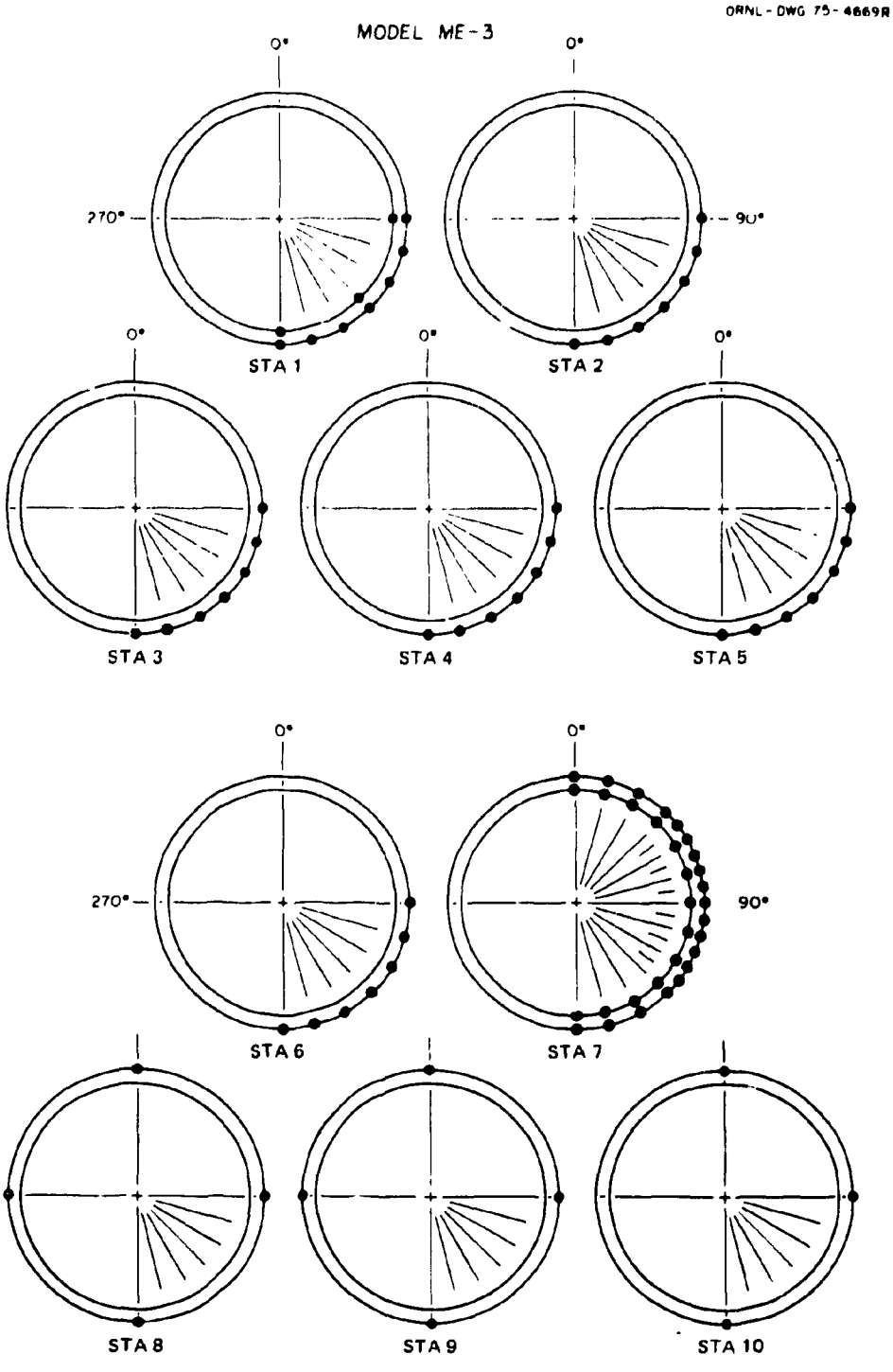

Fig. 2.9. Strain gage locations for test model ME-3.

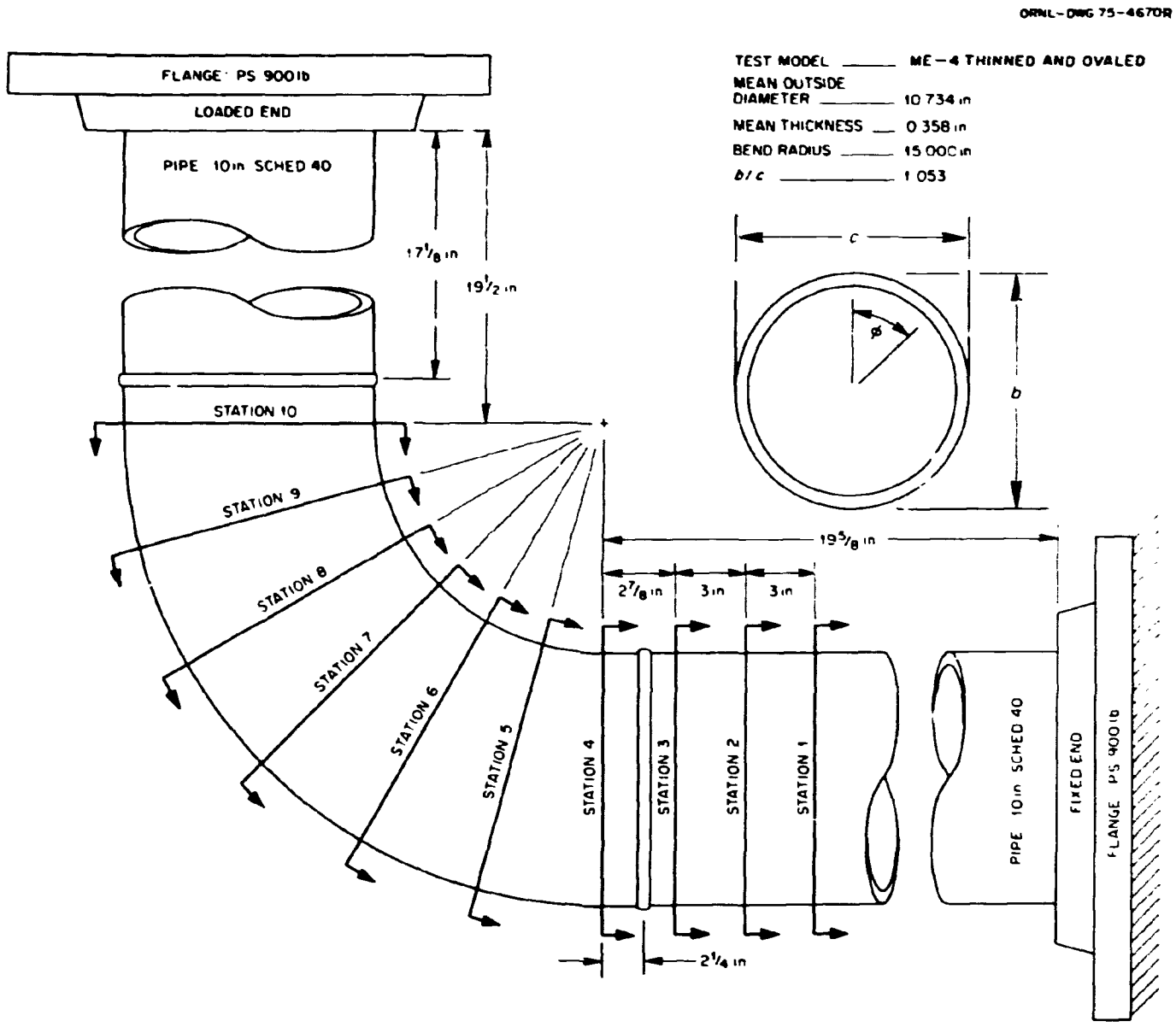

Fig. 2.10. Dimensional data for test model ME-4.

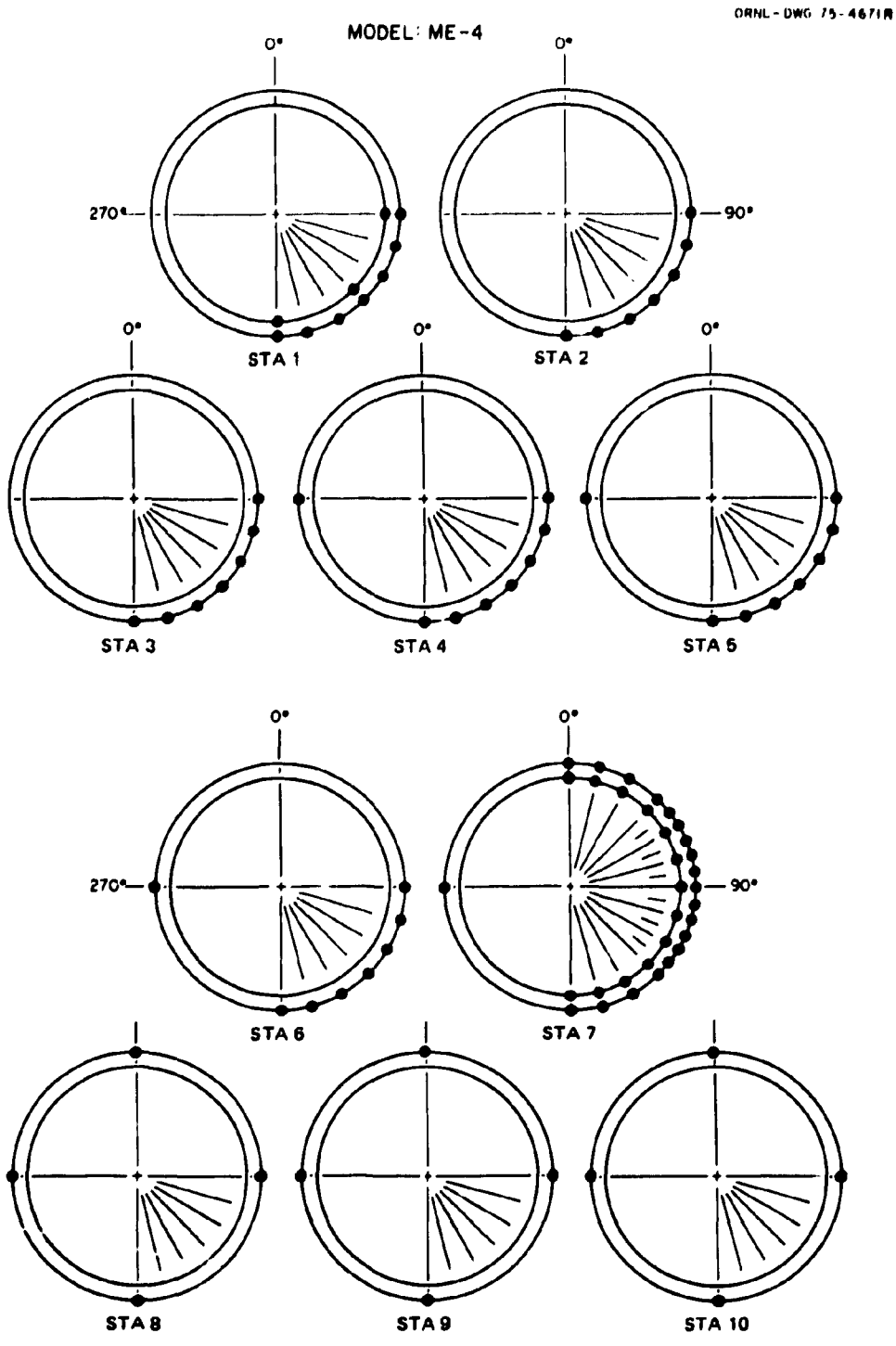

Fig. 2.11. Strain gage locations for test model ME-4.

ORNL PHOTO 79136A

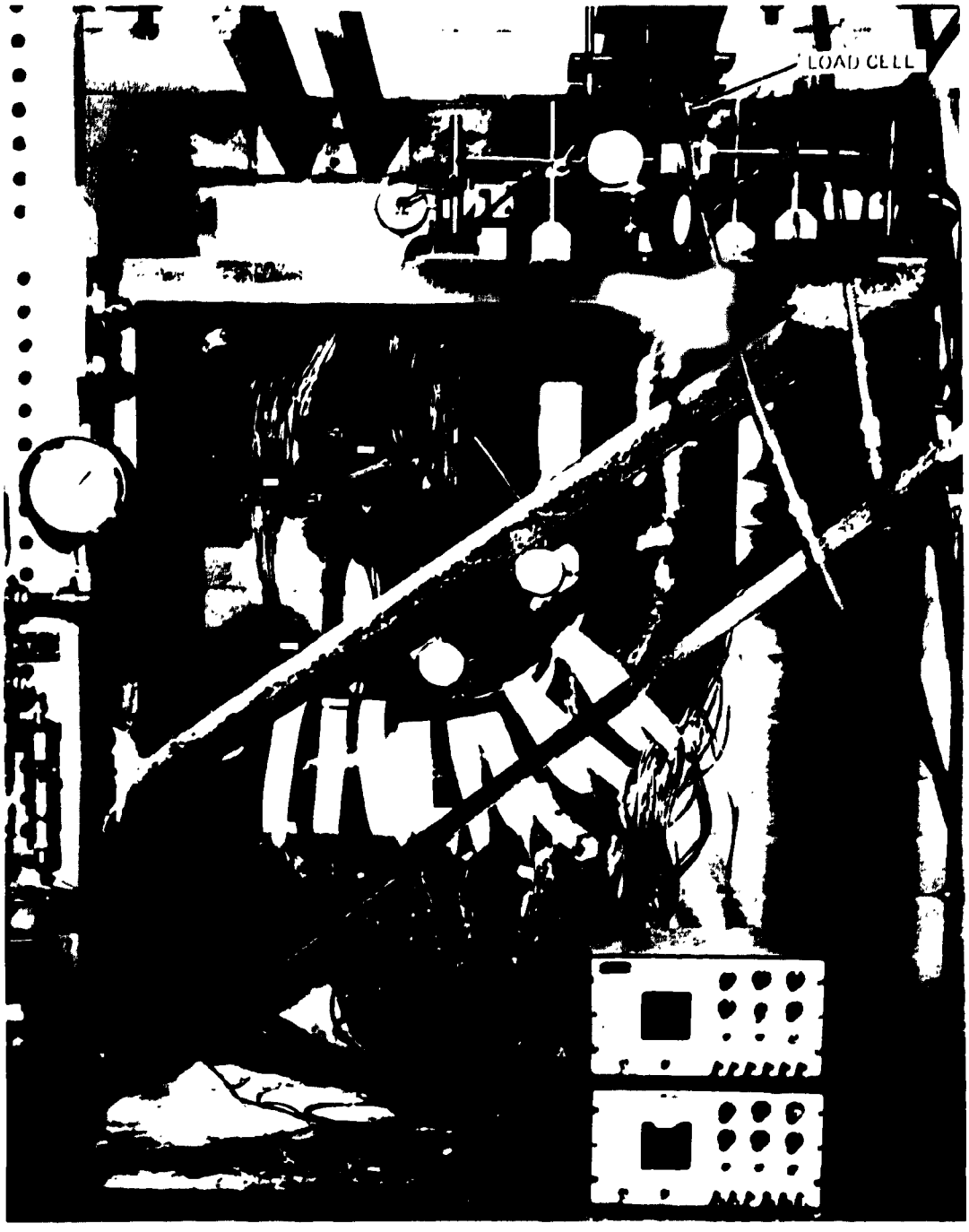

Fig. 2.12. Model ME-1 in the load frame with an out-of-plane moment loading being applied.

2.3 Test Setup

All of the models were tested in the load frame shown in Fig. 2.12. Overall the load frame was 5 ft 5 in. long, 5 ft high (extendable to 6 ft 8 in. high), and 4 ft 3 in. wide. The load frame was designed for application of loads in excess of 100,000 lb.

Each elbow test assembly was mounted in the load frame by bolting the class 900 slip-on flange at one end of the test assembly to a 2-in.-thick steel plate welded to the load frame. During moment-load testing, the loads were applied to the other end of the assembly by means of two matched hydraulic jacks that were mounted 28 in. apart on the cross beams of the loading frame shown in the upper part of Fig. 2.12. Great care was taken to align the jacks parallel and in a plane perpendicular to the test assembly so that pure bending loads would be applied. Load cells mounted in line with the hydraulic jacks were used to measure and balance the applied forces. The top of the test assembly was unrestrained during the internal pressure tests.

3. EXPERIMENTAL PROCEDURES

The elastic response (strain gage) tests and data reduction are described in this chapter. Evaluation of the data is discussed in the next chapter.

3.1 Elastic Response Tests

Elastic response strain gage tests were conducted on each of the four models for the following loadings: simple internal pressure; simple in-plane bending, out-of-plane bending, and torsional moment loads; and internal pressure combined with each of the three simple moment loads. The combined pressure-moment tests were conducted to examine the nonlinear character of the elbow response discussed by Rodabaugh and George.[4]

In the simple pressure and simple moment tests, a complete set of strain gage data was obtained at zero load and then at each of three equal loading increments up to the maximum. A small additional load was then applied so that new data could be obtained at the same load points during unloading. A second zero-load calibration test was then conducted and the strain gage data were checked for continuity, linearity, repeatability, and return to zero. If all of the data checked, the model was tested for the next load. If not, repairs were made where possible and the entire test was repeated. In general, however, it was not possible to repair inside-surface strain gages.

For the combined pressure-moment tests, a zero-load calibration test was first conducted as before. Internal pressure equal to one-third P_{max} was then applied, held constant, and a complete moment-loading sequence was conducted. The pressure was then raised to two-thirds P_{max} and the process was repeated. A similar test was conducted for the maximum pressure P_{max} and for the same pressure readings during unloading. Finally, the zero-load calibration test was repeated and the strain gage and load-cell data were checked before proceeding to the next pressure-moment series of tests.

Maximum loads for all of the tests are listed in Table 3.1. These loads were limited to values well within the elastic-response range,

Table 3.1. Maximum loads applied to elbow test models

Model	Simple loadings			
	Pressure (psi)	In-plane bending (in.-lb)	Out-of-plane bending (in.-lb)	Torsion (in.-lb)
ME-1	1,305	94,080	94,080	94,080
ME-2	600	188,160	188,160	188,160
ME-3	1,305	188,160	188,160	188,160
ME-4	600	188,160	188,160	188,160

	Combined loadings (psi/in.-lb)		
	Pressure/ in-plane bending	Pressure/ out-of-plane bending	Pressure/ torsion
ME-1	1,305/94,080	1,305/94,080	1,305/94,080
ME-2	600/188,160	600/188,160	600/188,160
ME-3	1,305/188,160	1,305/188,160	1,305/188,160
ME-4	600/188,160	600/188,160	400/188,160

generally to less than 1000 μin./in. for the highest strain reading. For pressure loadings, the maximum value for the circular-cross-section models ME-1 and ME-3 was 1,305 psi, which gave a maximum stress of about 20,000 psi. This was high enough to give good experimental resolution but well below the minimum yield strength so that the response should be linear with load. The maximum pressure for the ovaled models ME-2 and ME-4 was limited to 600 psi because of the higher stresses caused by the out of roundness.

The maximum moment loads for ME-1 were limited to 94,080 in.-lb. After this model was tested and the data were reduced, the maximum moment load for the other models was increased to 188,160 in.-lb to obtain better resolution for some of the smaller strain readings. The directions of the applied moment loadings conformed with the notation of Fig. 1.1, except for the torsional loadings on ME-1, which were in the opposite direction.

All of the strain gage and load cell data were recorded on a Datum Computer-Controlled Data Acquisition System. The system consists of a data acquisition module controlled by a PDP-8/I computer with the following capabilities: (1) magnetic tape input/output system, (2) in-core calculation ability for converting input signals to strain values, and (3) teletypewriter input and output. The unit had about 900 high-resolution input channels for strain data acquisition and additional lower resolution input channels for other data. Final load data and strain readings were stored on magnetic tape for processing at the ORNL computing center.

3.2 Data Reduction

As noted above, the strain data were checked for gage continuity, linearity with load, repeatability, and return to zero during the testing phase. After the tests were completed, the data were subjected to a rather exhaustive statistical diagnostic analysis to determine the "best" load-strain relation for each gage site. A diagnostic procedure described in Ref. 5 and the implementing computer program LINDA were used for this procedure. The procedure depends only on the hypothesis that strains obtained from a linear-elastic test are proportional to the loads. The procedure is therefore generally applicable to all tests of this type. Under the linear hypothesis, any nonlinearity in the data is considered to be due to errors either in measuring or in recording the strains or loads. The program LINDA identifies and distinguishes between the two types of errors.

In the first step, LINDA examines the data from each gage for load response linearity. Individual data points that do not pass an acceptance-tolerance-band test are identified and eliminated. The linearity tests are repeated until all the retained data are accepted.

In the next step, a load-variability test is conducted. Using a normalizing procedure, data from all the gages at each load step are examined for consistency within the data set. The mean normalized strains and their corresponding confidence intervals are used to estimate the most likely values for the applied loads and the corresponding confidence

bands. Out-of-tolerance data are identified and eliminated, and the process is repeated until the estimated mean loads and confidence bands converge. The processed load-strain data are then used to calculate normalized stresses (experimental stress indices) at each gage site using standard stress-strain-rosette formulas.[6] The nominal loads per 1000 psi stress are listed in Table 3.2.

Table 3.2. Nominal loads used in stress calculations

Model	Nominal loads[a]	
	Pressure (psi)	Moment (in.-lb)
ME-1	75.53	32,660
ME-2	74.24	32,270
ME-3	71.28	31,330
ME-4	69.01	30,270

[a]Nominal loads are normalized values corresponding to $Pr/t = M/\pi r^2 t = 1000$ psi, where P = pressure (psi), M = applied moment (in.-lb), r = elbow midsurface mean radius, and t = average wall thickness.

The calculated experimental stress indices from each test, identified by gage position, are tabulated in Appendix B. The values reported for the combined pressure-moment tests represent *only* the stresses from the applied moment loads. The pressure stresses were zeroed out during the data acquisition phase of the test. It is therefore possible to directly compare moment-load stresses for each model with and without pressure. If the total stresses are desired they can be obtained by direct addition.

4. EXPERIMENTAL RESULTS AND EVALUATION

As noted earlier, one objective of the present study was to obtain experimental data on the effects of out of roundness and wall-thickness variations to determine whether these effects may be important for design purposes. Because the stress distributions in elbows are unusually complex, and because the effects that may be specifically attributed to out of roundness and/or wall thinning were expected to be small, a substantial analytical effort was also necessary to isolate and evaluate the effects. To aid in this, a number of theoretical solutions — and associated computer programs — were used to analyze the test models. The analytical tools and the models and loadings that were analyzed are identified in Table 4.1. They include the theoretical membrane-stress solution for internal pressure of Lorenz;[7] the finite-element computer program EPACA;[8] the shell-theory computer program CURT-II,[9] adapted from work by Kalnins;[10] a theoretical solution for elliptical-cross-section elbows with either in-plane or out-of-plane moment loads by Findlay and Spence;[11] the no-end-effects (NEE) theory computer program ELBOW;[12,13] an asymptotic solution for elliptical elbows under internal pressure by Clark, Gilroy, and Reissner;[14] and Rodabaugh's treatment of out of roundness for internal pressure,[15] based on the work of Haigh[16] for straight pipe.

None of the above are able to completely describe the behavior of all four elbows with their attached pipe stubs. The widely used computer program ELBOW, for example, is based on von Karman's theory,[17] which assumes that deformations and stresses are constant along the length (i.e., end effects are neglected). The theories of Lorenz;[7] Findlay and Spence;[11] Clark, Gilroy, and Reissner;[14] and Rodabaugh[15] are also NEE theories. Recent studies by Rodabaugh and Moore,[18] however, show that the stresses and flexibilities of elbows welded to straight pipe and loaded with bending moments are not only a function of end effects but also of the elbow arc length. The computer programs CURT-II and EPACA are capable of treating end effects and arc length but are not able to consider out of roundness or variations in wall thickness.

Results for simple internal pressure on all four test models are discussed in Sect. 4.1. Simple in-plane moment loads are discussed in Sect.

Table 4.1. Models and loadings analyzed by various theoretical methods

Analytical method[a]	Loadings						
	Internal pressure	In-plane bending	Pressure/ in-plane bending	Out-of-plane bending	Pressure/ out-of-plane bending	Torsion	Pressure/ torsion
Lorenz	ME-1,2,3,4						
EPACA	ME-1	ME-1		ME-1			
CURT-II	ME-1	ME-1		ME-1			
Findlay and Spence		ME-2,4		ME-2,4			
ELBOW		ME-1,2,3,4	ME-1,2,3,4	ME-1,2,3,4	ME-1,2,3,4	ME-1,2,3,4	ME-1,2,3,4
[illegible], Gilroy, and [illegible]sner		ME-2,4					
Rodabaugh	ME-2,4						

[a]See text for references.

4.2, and simple out-of-plane and torsional moment loads are discussed in Sect. 4.3. Moment loads combined with internal pressure are discussed in Sect. 4.4. All of the stress data discussed in this chapter are given relative to nominal values (i.e., they are given as stress indices). The nominal stress for pressure is Pr/t and for moment loads is $M/\pi r^2 t$, where P and M are the nominal loads given in Table 3.2, and r and t are the mean radius and average wall thickness of the test models given in Table 2.1.

4.1 Simple Internal Pressure

Normalized experimental values for the longitudinal and circumferential stresses on the outside surface of the test models are shown in Figs. 4.1 and 4.2, respectively, for internal pressure loadings. From these figures it is readily apparent that the out of roundness in models ME-2 and ME-4 had a significant influence on the stresses [Figs. 4.1(*b*) and 4.2(*b*) and Figs. 4.1(*d*) and 4.2(*d*), respectively]. The wall-thickness variations in models ME-3 and ME-4, however, appear to have had very little influence [Figs. 4.1(*c*) and 4.2(*c*) and Figs. 4.1(*d*) and 4.2(*d*), respectively]. End effects appear to be significant only for the out-of-round elbows ME-2 and ME-4.

Figures 4.3 and 4.4 show comparisons of the experimental data at the elbow midsections (station 7) with analytical results from the membrane theory of Lorenz[7] and the out-of-round pipe theory of Rodabaugh.[15] Numerical values are summarized in Table 4.2. Both of the figures show very little difference between the inside-surface and outside-surface stresses for the circular-cross-section models ME-1 and ME-3, indicating the absence of significant shell bending. See Figs. 4.3(*a*) and 4.4(*a*) for ME-1 and Figs. 4.3(*c*) and 4.4(*c*) for ME-3. For these models, Lorenz theory (normalized to Pr/t),

$$\sigma_{\phi m} = \left[\frac{1 - 0.5(r/R)\cos\phi}{1 - (r/R)\cos\phi}\right], \tag{4.1}$$

$$\sigma_{\alpha m} = 0.5, \tag{4.2}$$

gives good overall agreement for both the longitudinal stresses and the

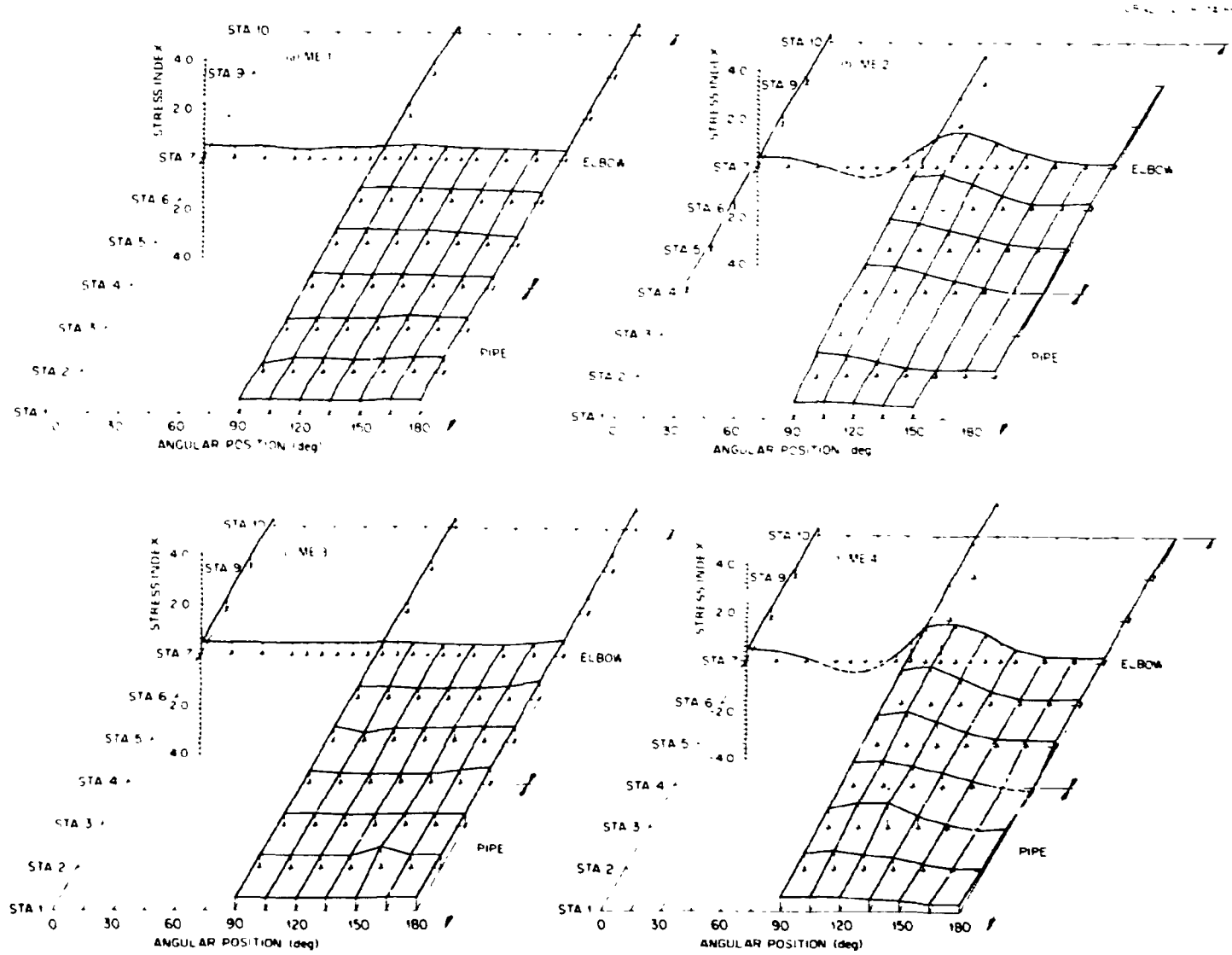

Fig. 4.1. Experimental normalized outside surface longitudinal stress distributions for each of the four test models loaded with internal pressure.

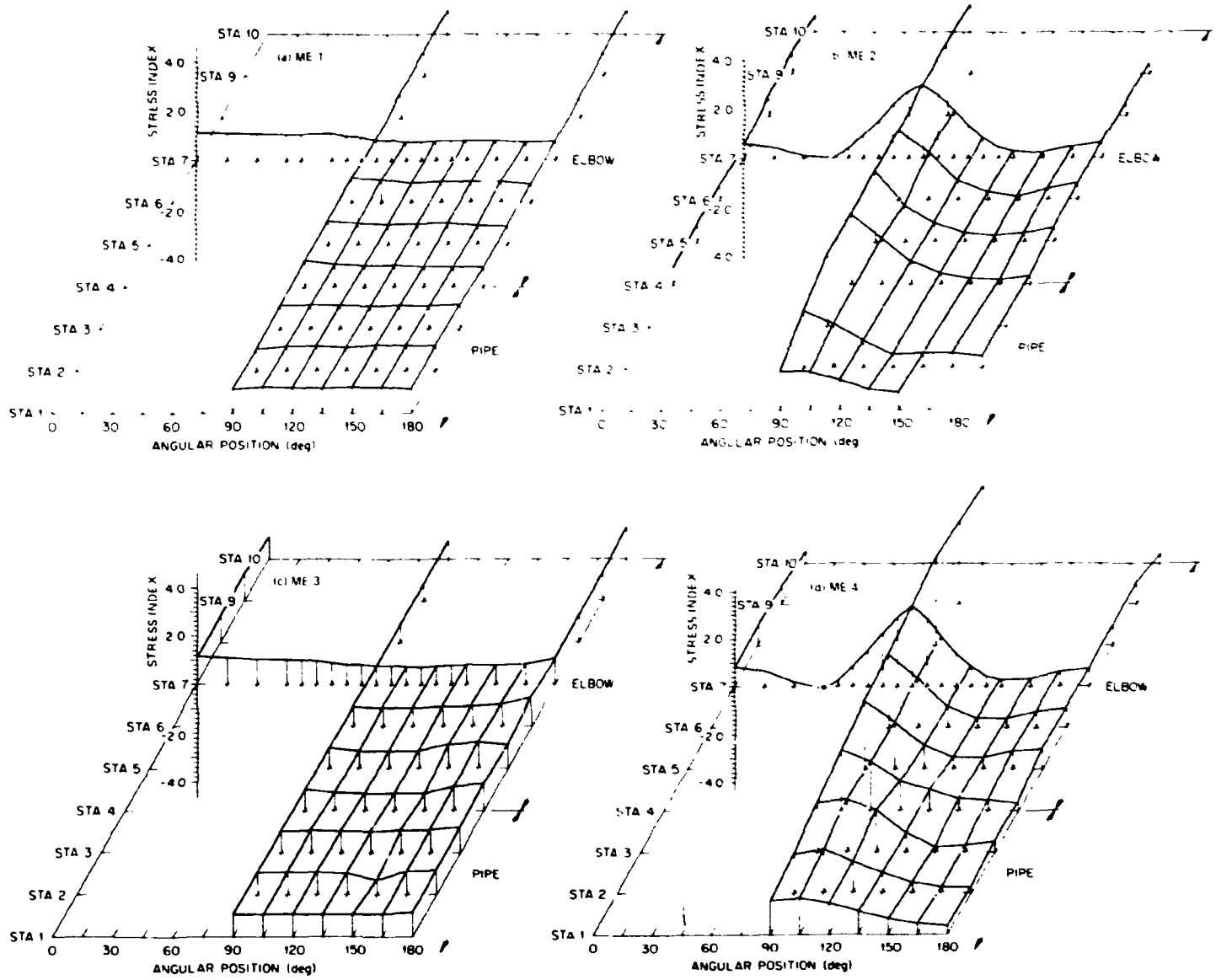

Fig. 4.2. Experimental normalized outside surface circumferential stress distributions for each of the four test models loaded with internal pressure.

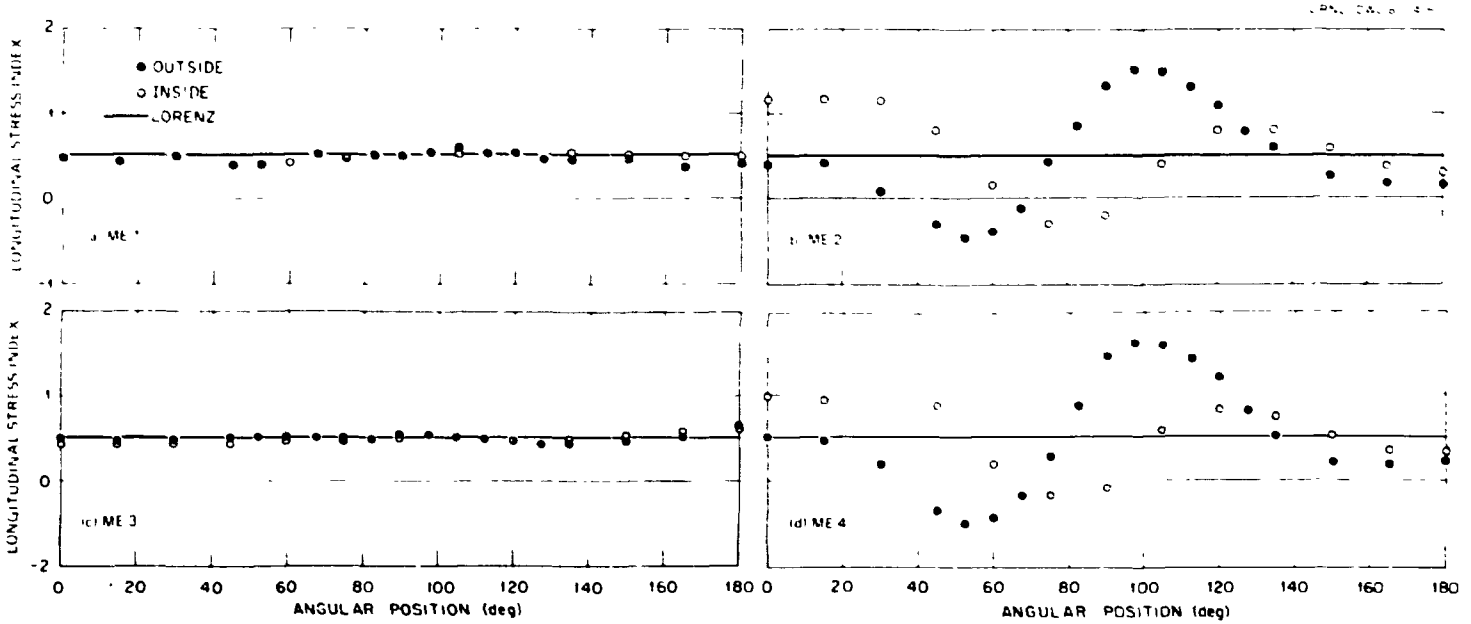

Fig. 4.3. Normalized longitudinal stresses at the elbow midsection (station 7) for each of the four test models loaded with internal pressure.

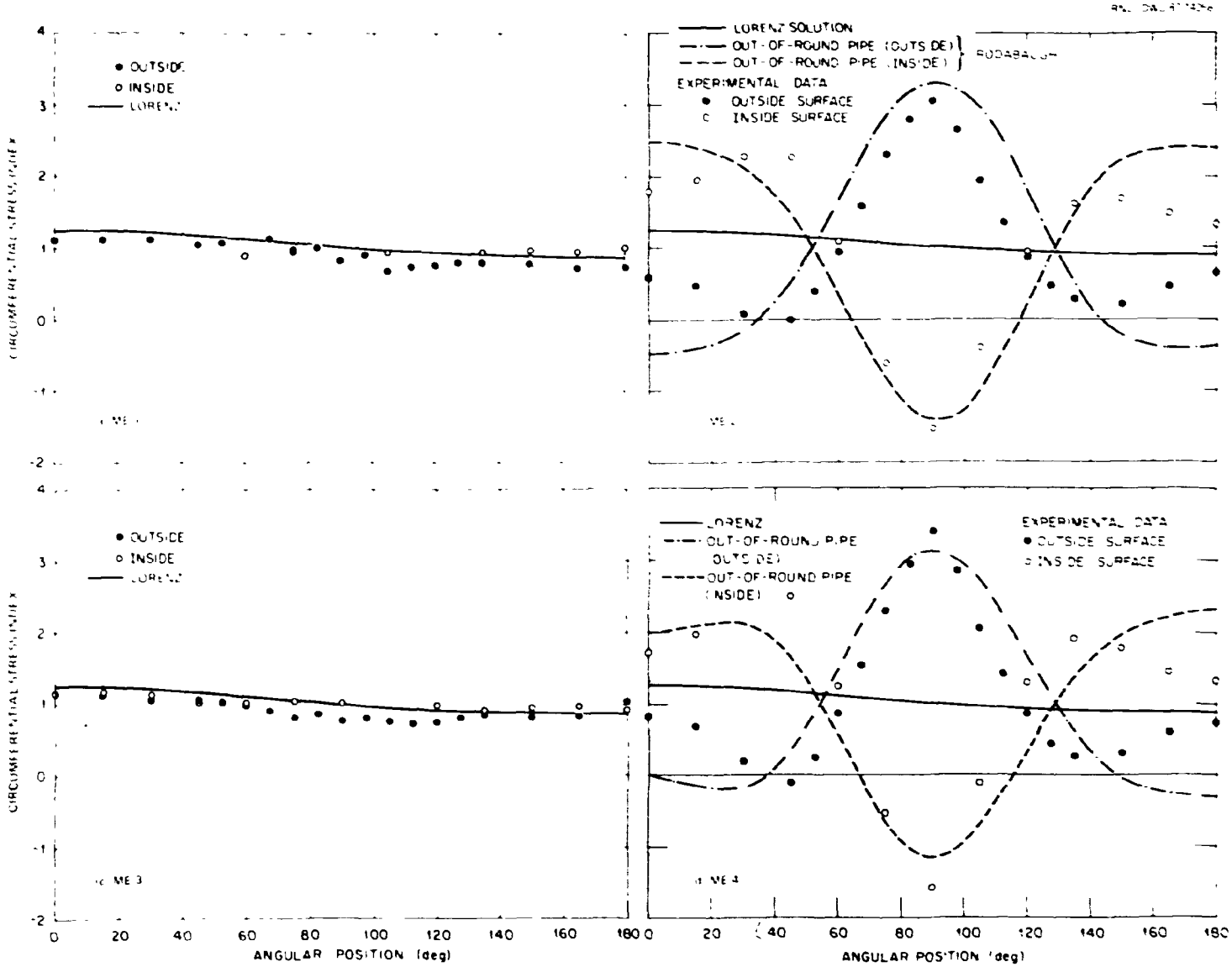

Fig. 4.4. Normalized circumferential stresses at the elbow midsection (station 7) for each of the four test models loaded with internal pressure.

Table 4.2. Maximum experimental and theoretical membrane-stress and bending-stress indices[a] at elbow midsections for simple internal pressure loads

Model	Experiment[b]				Theory[c]			
	$\sigma_{\phi m}$	$\sigma_{\alpha m}$	$\sigma_{\phi b}$	$\sigma_{\alpha b}$	$\sigma_{\phi m}$	$\sigma_{\alpha m}$	$\sigma_{\phi b}$	$\sigma_{\alpha b}$
ME-1	*d*	*d*	*d*	*d*	1.00	0.50	0.27	*e*
ME-2	0.76	0.56	2.29	0.76	1.00	0.50	2.22	*e*
ME-3	0.90	0.49	0.12	0.03	1.00	0.50	0.42	*e*
ME-4	0.91	0.68	2.49	0.77	1.00	0.50	2.10	*e*

[a] Internal pressure stresses normalized to $PD_m/2t$, where P is the nominal pressure given in Table 3.2, D_m is the mean diameter, and t is the average wall thickness, given in Table 2.1. Symbols: $\sigma_{\phi m}$ = circumferential membrane-stress index; $\sigma_{\alpha m}$ = longitudinal membrane-stress index; $\sigma_{\phi b}$ = circumferential shell-bending-stress index; $\sigma_{\alpha b}$ = longitudinal shell-bending-stress index.

[b] For detailed experimental data see Appendix B.

[c] Theoretical membrane-stress indices from Eqs. (4.1) and (4.2) and circumferential bending-stress indices from Eq. (4.3) evaluated at $\phi = 90°$. Theoretical bending-stress indices from Eq. (4.5).

[d] Experimental membrane and bending stresses were not obtained for ME-1 because the inside surface gage at $\phi = 90°$ failed prior to the test.

[e] Rodabaugh[11] does not give an expression for the longitudinal bending stress.

circumferential stresses, although, as shown in Table 4.2, the maximum circumferential stress was somewhat less than predicted by the theory. Equation (4.1), evaluated at $\phi = 0°$, is the ASME Code equation for the stress index C_1 for nuclear Class 1 butt-welding elbows or curved pipe (see NB-3683.7).

On the other hand, the figures for the out-of-round models ME-2 and ME-4 show a considerable amount of shell bending in both the longitudinal and circumferential directions [see Figs. 4.3(*b*) and (*d*) and 4.4(*b*) and (*d*)]. For these models, Rodabaugh's theory (normalized to Pr/t),

$$\sigma_{\phi b} = \pm \frac{6}{t} \sum_{n=2}^{k} \frac{A_n \cos n\phi + C_n \sin n\phi}{1 + J_n} , \qquad (4.3)$$

where

$$J_n = \frac{12\ (1 - \nu^2)}{(n^2 - 1)} \left(\frac{D_m}{2t}\right)^2 \left(\frac{P}{E}\right), \tag{4.4}$$

represents the maximum circumferential bending stress at about $\phi = 90°$ reasonably well but does not accurately represent the bending stress all the way around the circumference. This is to be expected because Ref. 15 does not include the effects of bend curvature. Consequently, the discrepancy could be expected to be greater for elbows with a shorter bend radius (i.e, $r/R < 3$) and less for elbows or pipe bends with $r/R > 3$. Rodabaugh[15] does not give an expression for the axial-direction shell-bending stress $\sigma_{\alpha b}$.

The dashed lines shown in Fig. 4.4(*b*) and (*d*) for the theoretical circumferential stresses (Rodabaugh) were obtained by evaluating six terms of the series in Eq. (4.3), with $C_n = 0$ because of symmetry about $\phi = 0°$. Equation (4.3), evaluated for an "elliptical" cross section at $\phi = 0°$ and with $\nu = 0.3$,

$$\sigma_{\phi b} = \pm \left(\frac{D_{max} - D_{min}}{t}\right) \left(\frac{1.5}{1 + 0.455\ (D_m/t)^2\ (P/E)}\right), \tag{4.5}$$

plus the membrane-stress $\sigma_{\psi m}$ is the ASME Code equation for the peak-stress index K_1 for elbows or bends with out of roundness greater than $0.08(t/D_o)$ [see NB-3683.2(b)(1)]. The numerical values in Table 4.2 show good agreement between the experimental and theoretical bending stress indices ($\sigma_{\phi b}$), although Eq. (4.5) gives somewhat lower values (3 and 16%) than those measured for the out-of-round models ME-2 and ME-4. The theoretical values are somewhat higher than the experimental values for models ME-1 and ME-3. However, for these models the shell-bending stress is not significant.

The asymptotic solution of Clark, Gilroy, and Reissner[14] for elliptical-cross-section toroidal shells gave poor results for both ME-2 and ME-4. We did not attempt to evaluate their series solution.

Analytical results for ME-1 under internal pressure were also obtained with the finite-element computer program EPACA[8] and with the axisymmetric shell theory program CURT-II.[9] Neither of these programs were

capable of modeling out of roundness or wall thinning, although in principal special mesh generators could have been written for EPACA. In any case, it was not practicable to analyze ME-2, -3, or -4 with these programs. Comparative results from EPACA for ME-1 at station 7 are shown in Fig. 4.5. Outside-surface experimental stress indices at all seven stations are compared with the CURT-II analytical results in Fig. 4.6. Both programs gave excellent comparisons.

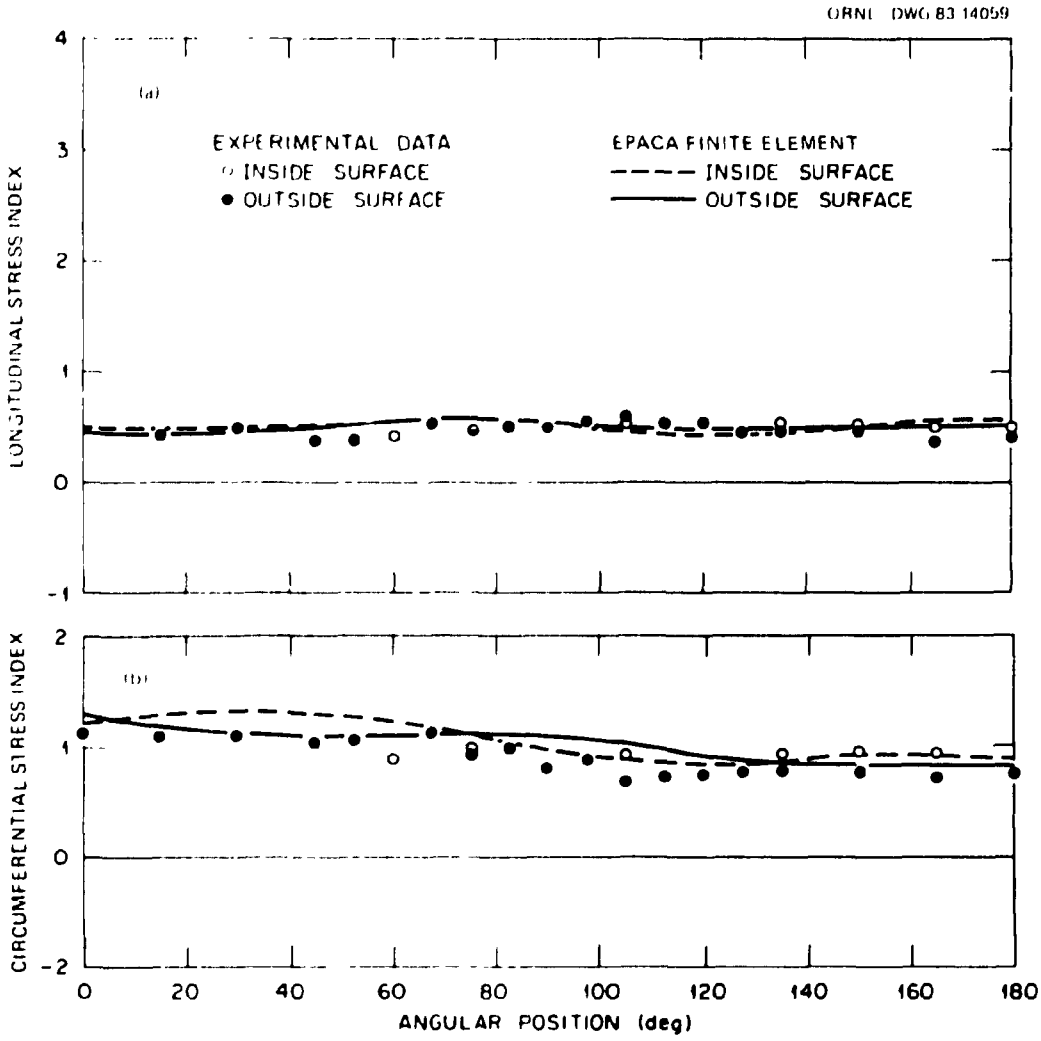

Fig. 4.5. Comparisons between EPACA finite-element and experimental results for model ME-1 loaded with internal pressure.

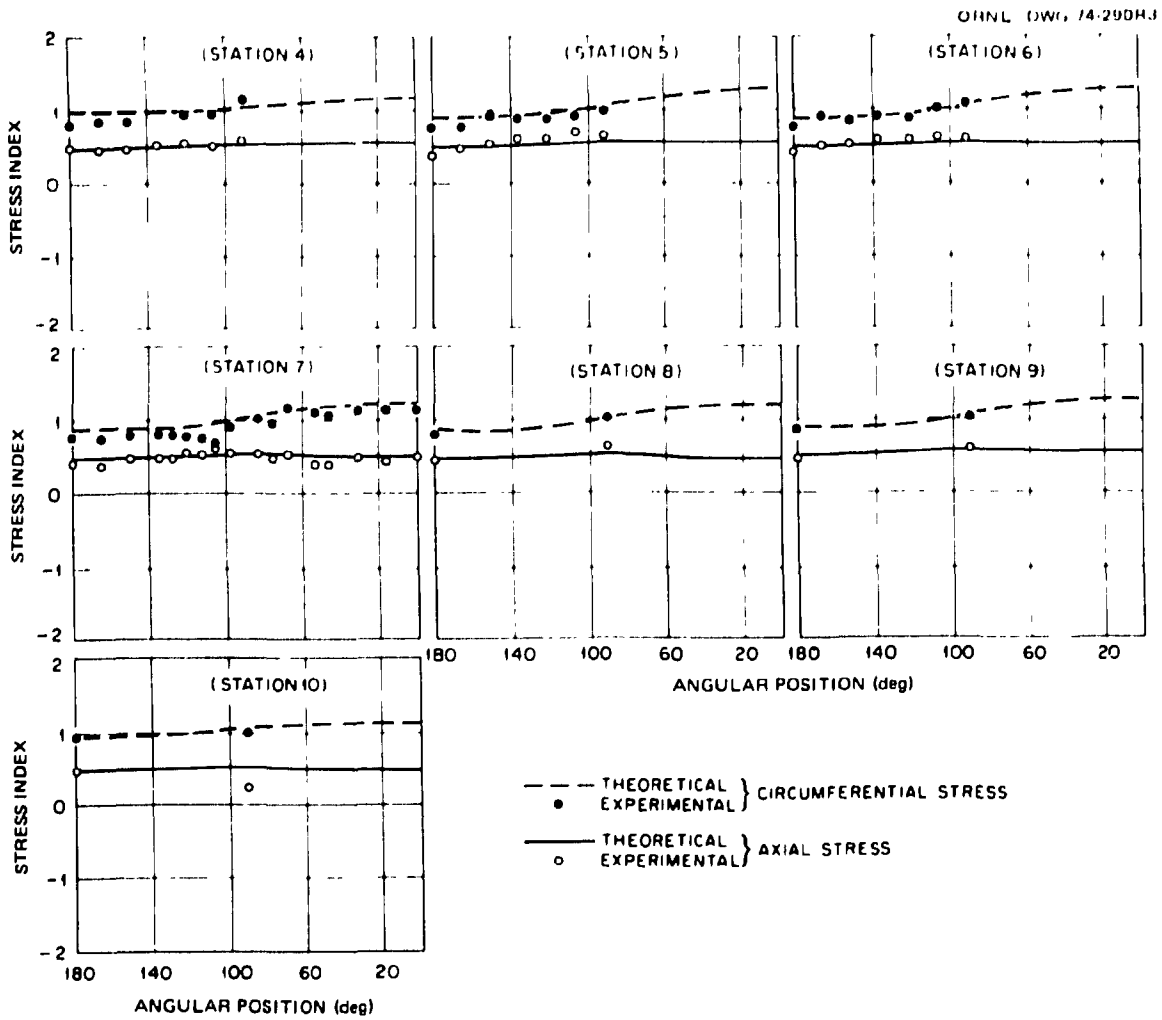

Fig. 4.6. Comparisons between CURT-II shell theory and experimental results for the outside surface of model ME-1 loaded with internal pressure.

4.2 Simple In-Plane Bending

Normalized experimental values for the axial and circumferential stress on the outside surface due to in-plane moment loads M_i are shown in Figs. 4.7 and 4.8, respectively. From these figures it is readily apparent that end effects reduce the magnitudes of the stresses significantly near the ends of the elbow. The shapes of the stress distributions around the circumference also change as a function of axial position, with

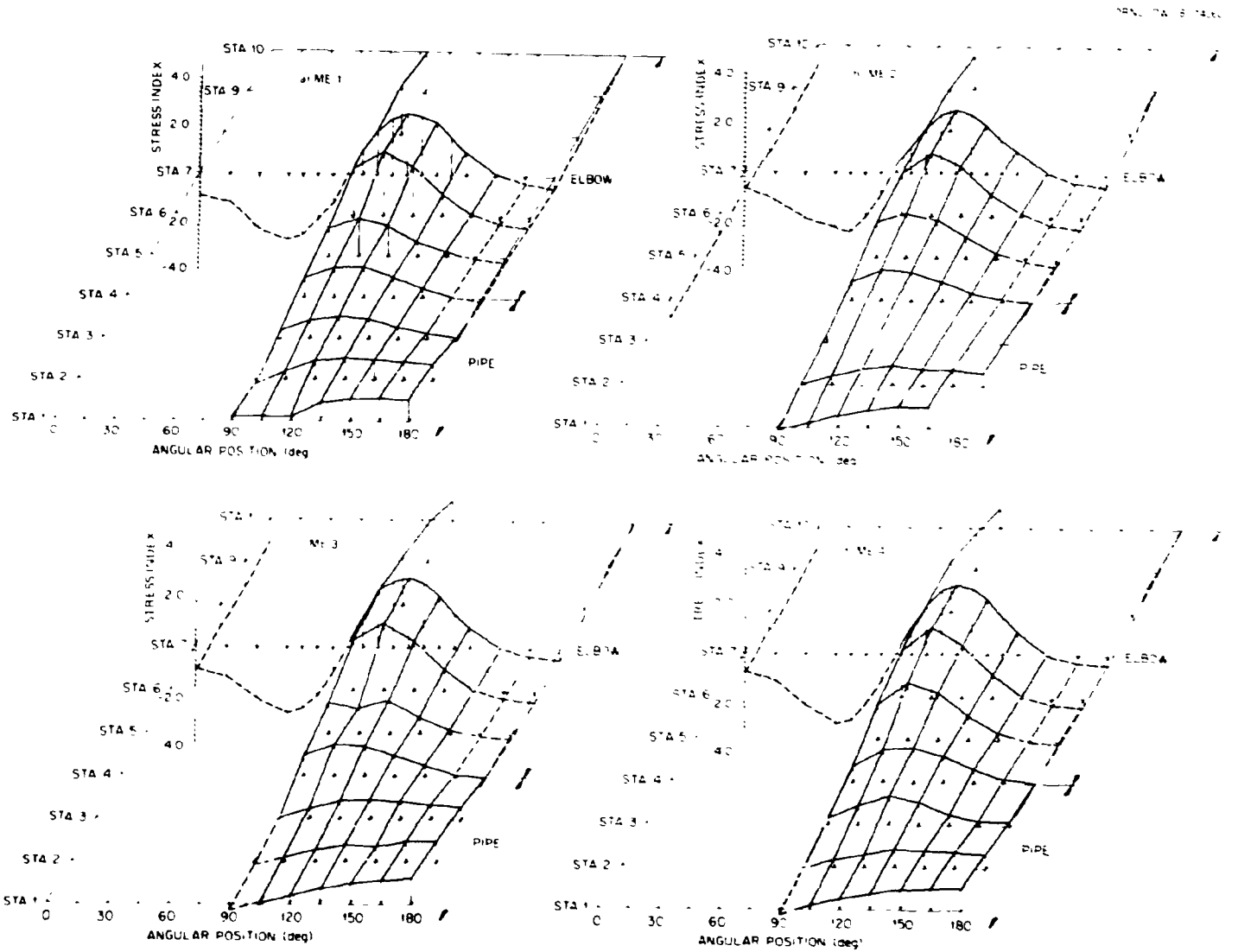

Fig. 4.7. Experimental normalized outside surface longitudinal stress distributions for each of the four test models loaded with a simple in-plane moment M_i.

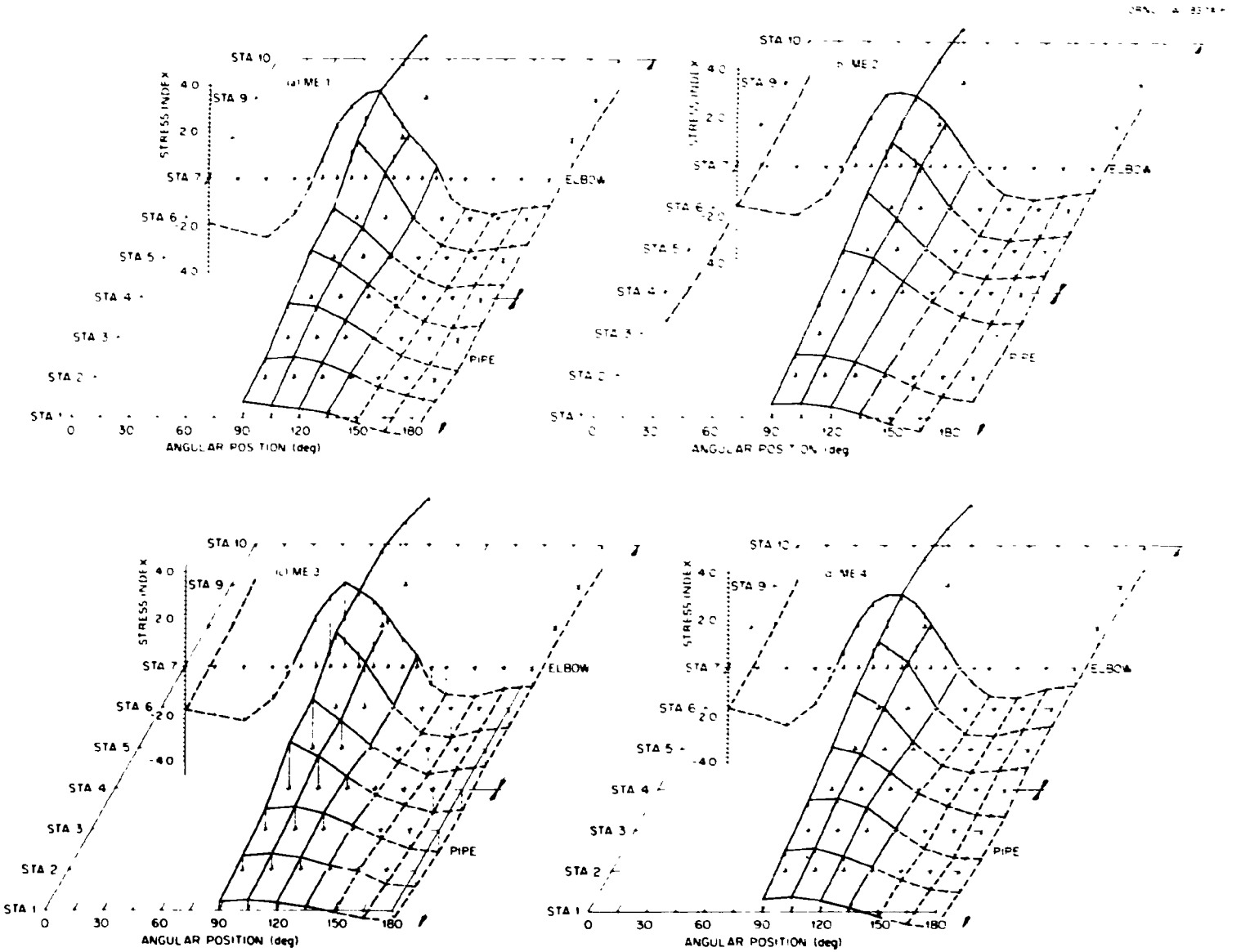

Fig. 4.8. Experimental normalized outside surface circumferential stress distributions for each of the four test models loaded with a simple in-plane moment M_i.

the maximum axial stress moving from the sides of the elbows, near ϕ = 100° at the midsection of the elbow, to the top at ϕ = 180° in the pipe stubs (Fig. 4.7). The location of maximum circumferential stress also appears to shift slightly from about ϕ = 80 or 85° at the center of the elbow (station 7) to ϕ = 90° in the pipe stubs (Fig. 4.8). The general shape of the stress distributions for all four models, however, appears remarkably similar.

Figures 4.9 and 4.10 show comparisons between the experimental data at the elbow midsections for all four models and the uniform-wall, circular-cross-section, NEE theory results from ELBOW. From Figs. 4.9(*a*) and 4.10(*a*) for ME-1, it may be inferred that end effects have only a small influence on the maximum stresses caused by in-plane bending in a geometrically perfect 90° elbow. This conclusion agrees with recent finite-element parameter studies of elbows of various arc lengths welded to long sections of straight pipe.[18] Figure 4.11 shows comparisons between the experimental data for the outside surface of ME-1 and the CURT-II shell theory analysis, which includes end effects but not out of roundness or wall thinning. The excellent agreement between the experimental and analytical results in Fig. 4.11 gives further evidence that the reduction in maximum stresses for ME-1 [Figs. 4.9(*a*) and 4.10(*a*)] is mainly the result of end effects.

It is not so easy to infer the effects of out of roundness or wall thinning on the stresses due to in-plane bending. The comparison of Fig. 4.9(*b*), (*c*), and (*d*) for ME-2, -3, and -4, respectively, indicates that neither out of roundness nor wall thinning had any significant influence on the axial stresses, because the differences between the experimental and analytical results appear to be about the same as for ME-1 [Fig. 4.9(*a*)]. On the other hand, the comparisons shown in Fig. 4.10 indicate that both out of roundness and wall thinning had a significant influence on the maximum circumferential stresses and hence on the design stress index. A quantitative assessment is given in Table 4.3.

The values shown in Table 4.3 for ME-2 and ME-4 are substantially less than predicted by available theoretical solutions — on the order of 20%. Both Findlay and Spence[11] and Clark, Gilroy, and Reissner[14] give NEE-

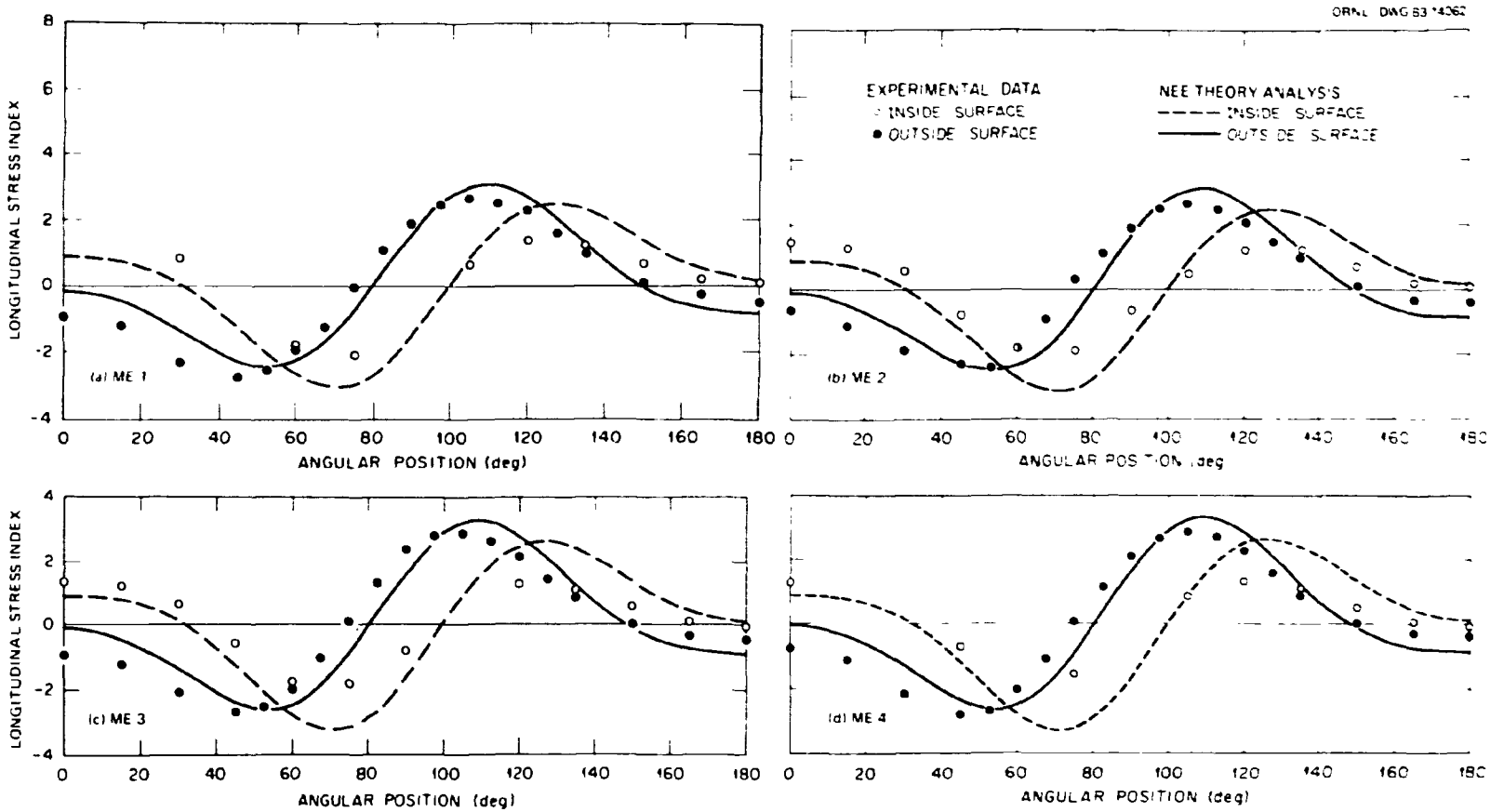

Fig. 4.9. Normalized longitudinal stresses at the elbow midsection (station 7) for each of the four test models loaded with a simple in-plane moment M_i.

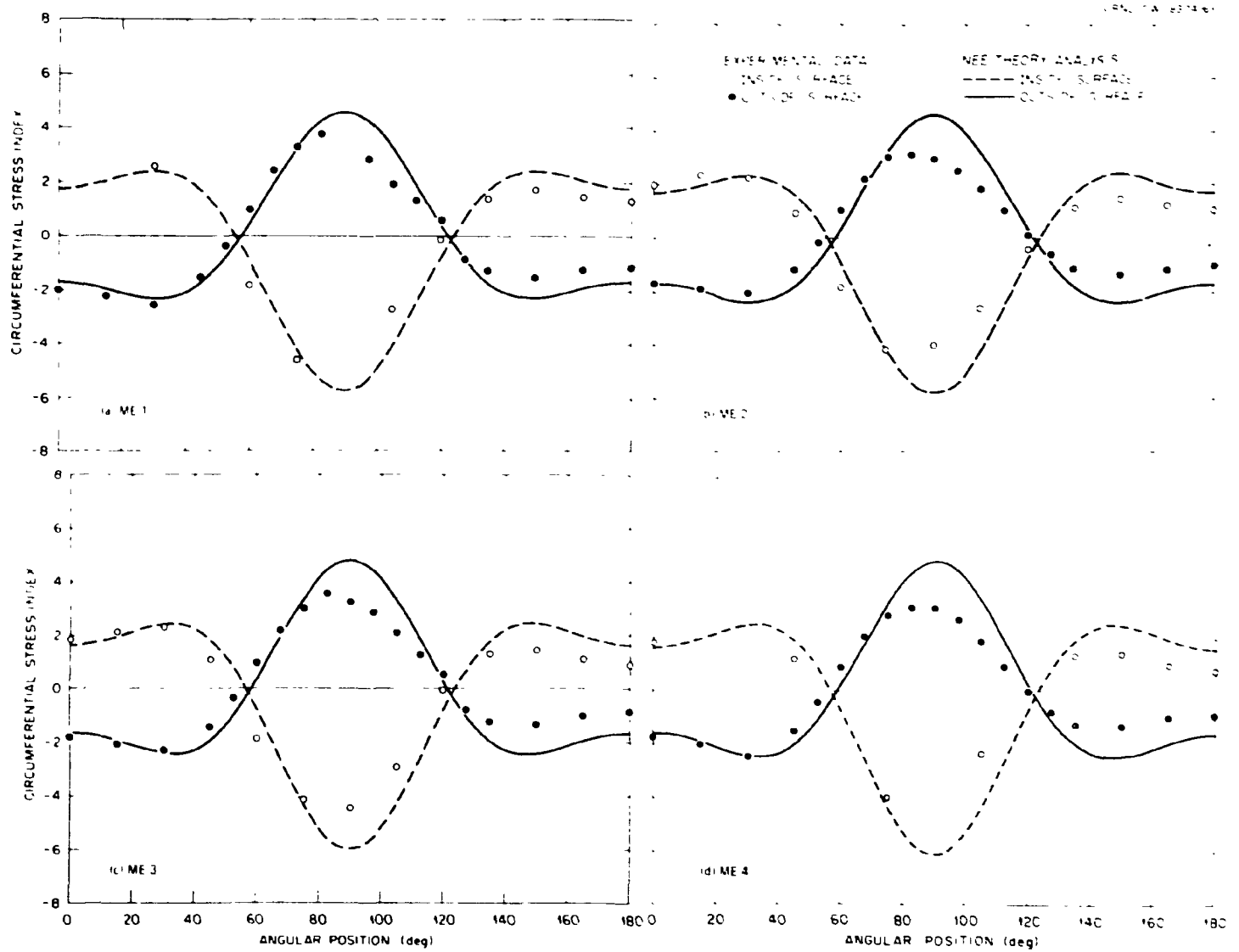

Fig. 4.10. Normalized circumferential stress at the elbow midsection (station 7) for each of the four test models loaded with a simple in-plane moment M_i.

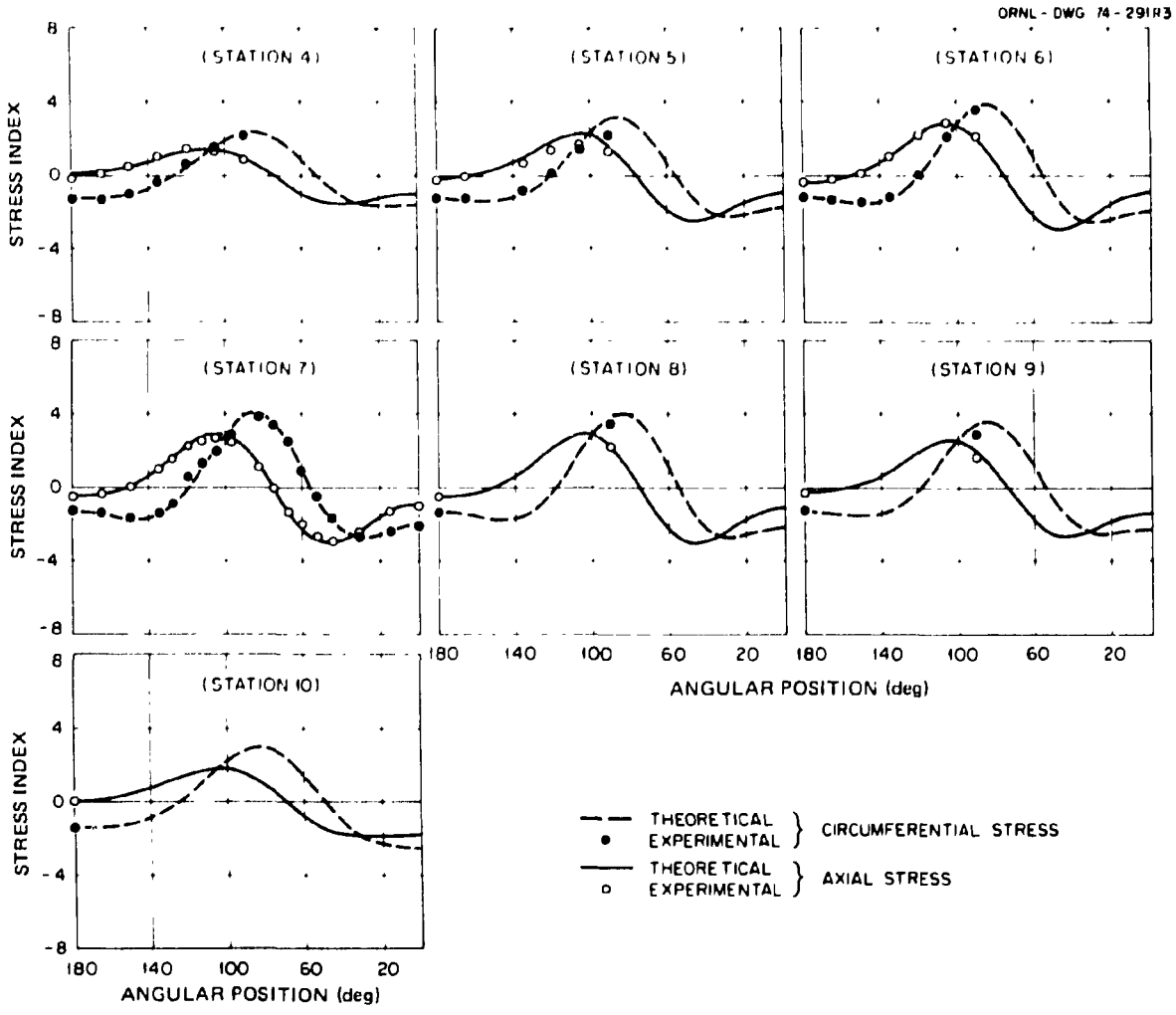

Fig. 4.11. Comparisons between CURT-II shell theory and experimental results for the outside surface of model ME-1 loaded with a simple in-plane moment M_i.

theory solutions for elliptical-cross-section elbows under in-plane bending. For out-of-round elbows with eccentricity on the order of 1, Findlay and Spence[11] give the maximum stress index for in-plane bending as

$$C_2' = \frac{\pi}{4\, B_1(\phi)} \frac{(1 + b/c)^2}{(b/c)} C_2 \,, \qquad (4.6)$$

where (b/c) is the ratio of the in-plane to out-of-plane cross-section diameters, C_2 is the in-plane bending-moment stress index for round elbows,

Table 4.3. In-plane moment stress indices at elbow midsection

Model	In-plane moment, inside surface at elbow midsection		
	NEE theory[a]	Experiment station 7[b]	Reduction (%)
ME-1	5.66	5.45	3.7
ME-2	5.73	4.50	21.5
ME-3	5.91	4.65	18.8
ME-4	6.03	4.40	27.0

[a]NEE theory indicates no end effects as exemplified by the von Karman theory and the ELBOW computer program.

[b]These values were estimated by interpolation between adjacent gage sites since the maximum values did not occur at $\phi = 90°$ (see Fig. 4.10). The value for ME-1 may be less accurate because the gage at $\phi = 90°$ failed before the test was conducted.

and $B_1(\phi)$ is the function

$$B_1(\phi) = \int_0^{2\pi} \frac{(b/c)^4 \sin^2 \phi}{(1 - e^2 \sin^2 \phi)^{5/2}} \, d\phi \, , \tag{4.7}$$

where eccentricity e is given by

$$e^2 = 1 - (b/c)^2 \, . \tag{4.8}$$

For elbows like ME-2 and ME-4 with about 5% out of roundness (i.e., b/c = 1.05), Eq. (4.6) gives $C_2' = 0.988\ C_2$, or less than 2% reduction in the maximum stress. This is considerably less than the 20% observed experimentally.

At this point, we can only surmise that end effects, which are not included in the theories of Refs. 11 and 14, interact with out of roundness and/or wall thinning in such a way as to alter the stress distributions around the circumference of the elbows, as indicated by the experimental data. Although a 20% *reduction* in maximum stresses may be only of

academic interest, if the eccentricity should occur in the opposite direction (i.e., b/c < 1.0) as is more likely for commercial elbows and pipe bends, then one might expect a substantial *increase* in the maximum stress. Additional research needs to be done to clarify this point.

For 90° elbows welded to long straight pipe, the major influence of end-effects is a significant reduction in the maximum stresses at the ends of the elbow. These effects are clearly evident in the experimental data shown in Figs. 4.7 and 4.8 and in the CURT-II analysis of ME-1 shown in Fig. 4.11. These figures indicate that the maximum stresses at the elbow-to-pipe junctions are only about half the values at the elbow midsections. A finite-element analysis of ME-1 with EPACA gave essentially the same results as CURT-II.

Table 4.4 gives a comparison between the maximum stress indices predicted by NEE theory and the experimental values at the elbow ends. As

Table 4.4. In-plane moment stress indices at elbow ends

Model	Stress index		
	NEE theory	Experiment station 4[a]	Reduction (%)[b]
ME-1	5.66	2.18	61.5
ME-2	5.73	2.06	64.0
ME-3	5.91	2.13	63.9
ME-4	6.03	1.93	68.0

[a]The analytical EPACA and CURT-II results showed that the outside-surface circumferential stresses are only slightly lower than the inside-surface stresses, indicating very little shell bending at the elbow ends. Since inside-surface stresses were not measured at this location, the outside-surface stresses are used for comparison.

[b]These percentage values should be reduced by about 5% to account for shell bending.

noted, the effect of the end restraint from the pipe stubs is to reduce the NEE theory stresses by about 60% for all four models. The data in Table 4.4 also indicate that out of roundness and wall thinning have very little influence on the maximum stresses at the elbow-to-pipe junctions.

4.3 Simple Out-of-Plane Bending and Torsion

Simple out-of-plane bending and torsional moment loads are discussed together in this section because they are reciprocal loads. For 90° elbows, an out-of-plane moment M_o applied at one end will be resisted by a pure torsional moment M_t at the other end. Conversely, an applied torsional moment will be resisted by a pure out-of-plane bending moment. At a given cross section, the magnitudes of the out-of-plane and torsional moment vectors $\bar{M}_o$ and $\bar{M}_t$ are given by

$$\bar{M}_o = M_o \cos \alpha + M_t \sin \alpha \,, \tag{4.9}$$

$$\bar{M}_t = M_o \sin \alpha + M_t \cos \alpha \,, \tag{4.10}$$

where α is the longitudinal angle in the plane of the bend and M_o and M_t are the magnitudes of the moments applied at the end $\alpha = 0$.

At the elbow midsection, $\alpha = 45°$, the magnitudes of the load vectors $\bar{M}_o$ and $\bar{M}_t$ will be the same whether the applied loading is out-of-plane bending M_o or torsion M_t. In addition, if the shapes of the cross sections are symmetrical about the midsection, then NEE theory and Eqs. (4.9) and (4.10) imply that the stress distributions around the elbow will be antisymmetrical about $\alpha = 45°$. This then implies that the stresses at $\alpha = 45°$ will be identical for M_o and M_t loads, except for a possible difference in sign ($\pm$) because of the direction of loading. For other cross sections (i.e., at $\alpha = 45 \pm \xi$) the stresses caused by M_t or M_o acting alone will be the same as those from M_o or M_t at $\alpha = 45 \mp \xi$ (except, perhaps, for the sign).

Figures 4.12–4.15 show the experimental outside surface stresses for both out-of-plane bending and torsional loads normalized to the value of M_o and M_t given earlier in Table 3.2. The corresponding experimental data

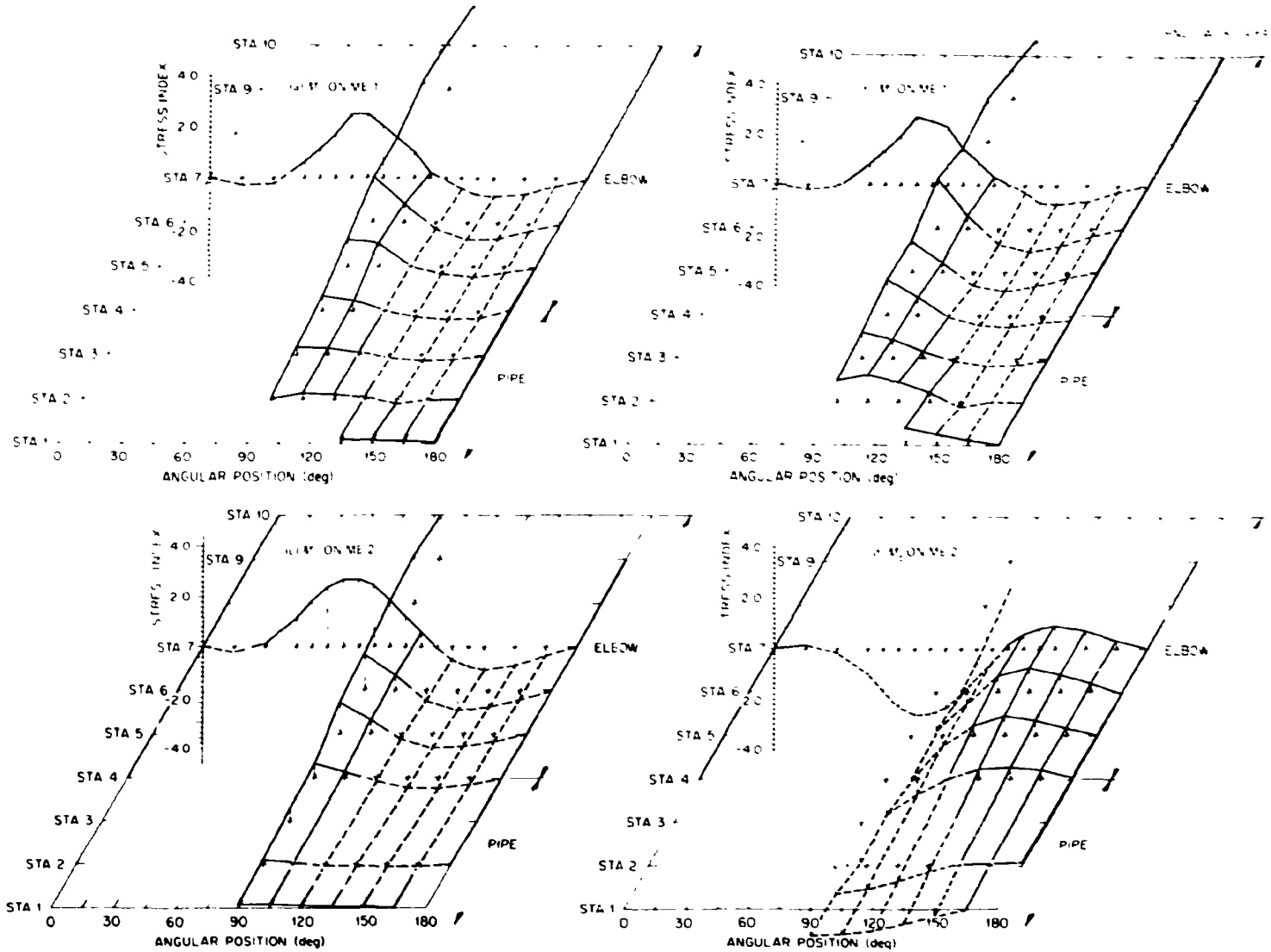

Fig. 4.12. Experimental normalized outside surface longitudinal stress distributions for models ME-1 and ME-2 loaded with out-of-plane (M_o) and torsional (M_t) moments.

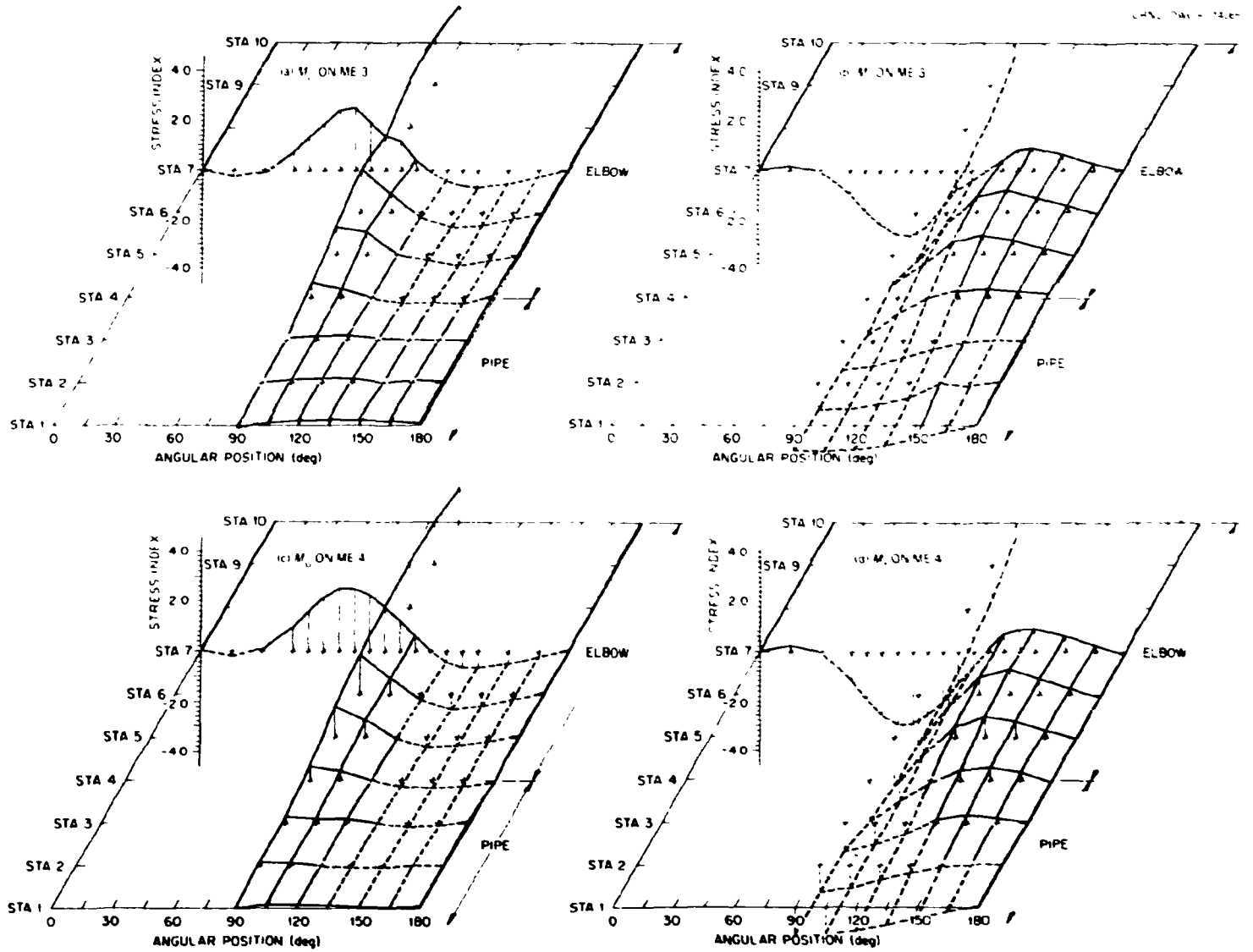

Fig. 4.13. Experimental normalized outside surface longitudinal stress distributions for models ME-3 and ME-4 loaded with out-of-plane (M_o) and torsional (M_t) moments.

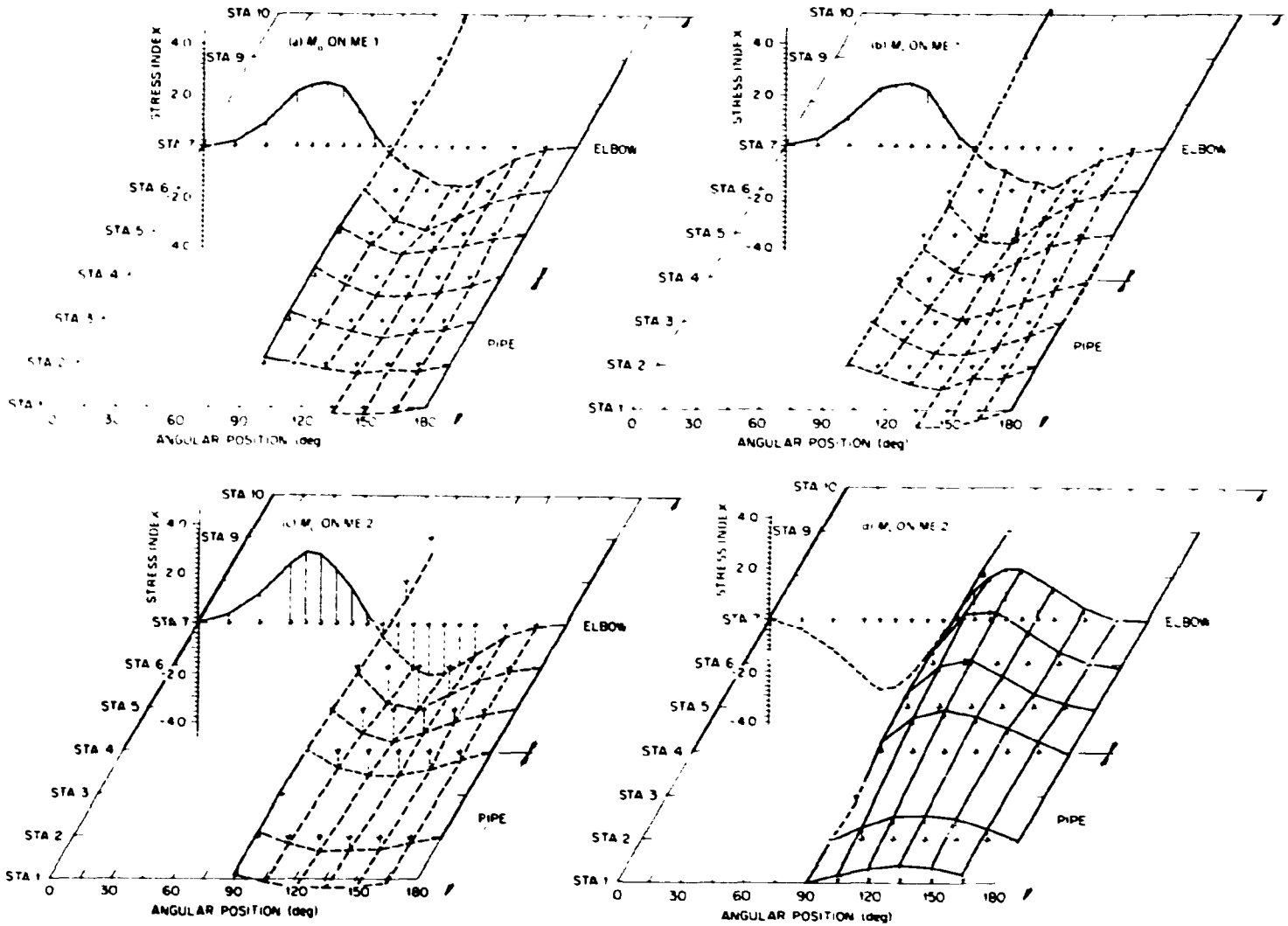

Fig. 4.14. Experimental normalized outside surface circumferential stress distributions for models ME-1 and ME-2 loaded with out-of-plane (M_o) and torsional (M_t) moments.

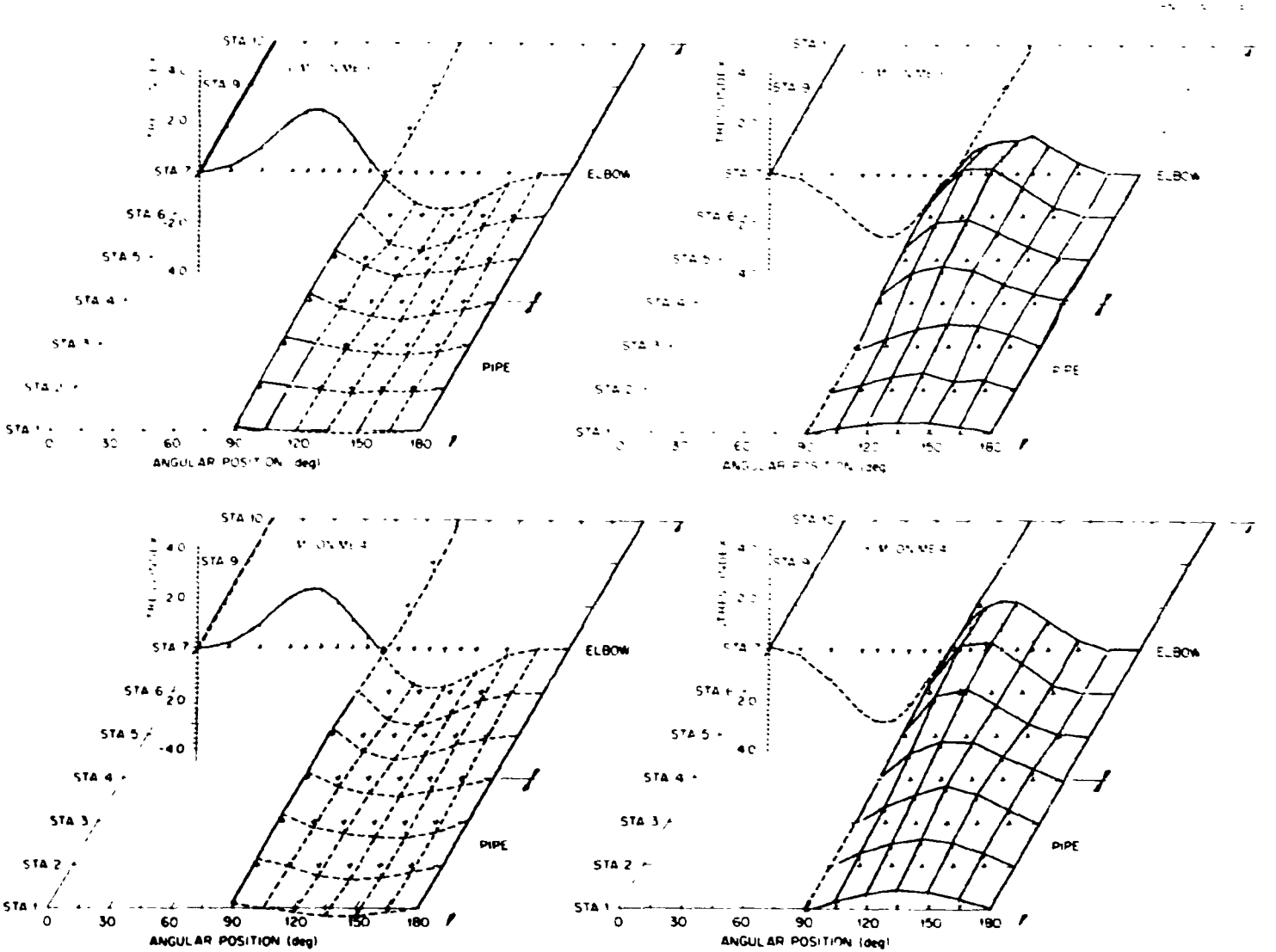

Fig. 4.15. Experimental normalized outside surface circumferential stress distributions for models ME-3 and ME-4 loaded with out-of-plane (M_o) and torsional (M_t) moments.

are tabulated in Appendix B. The upper part of Fig. 4.12 shows longitudinal stress indices for model ME-1 due to M_o on the left and stress indices due to M_t on the right. The lower part of the figure shows similar stress index distributions for ME-2. Longitudinal stress indices for ME-3 and ME-4 are shown in Fig. 4.13. Similar comparisons for the circumferential stresses are shown in Figs. 4.14 and 4.15.

Two things are immediately apparent from these figures. As expected, the stress distributions due to M_o and M_t are quite similar. Except for sign differences, the stresses appear to be almost identical, especially at the midsections. Table 4.5 is a listing of the experimental maximum values at station 7 for all four models under both M_o and M_t loadings. As may be seen, the maximum values from M_o and M_t for a given model differ only in sign because of the direction of applied loading. In addition, the values for the various stress components, $\sigma_{\alpha o}$, $\sigma_{\alpha i}$, etc., are about the same for each of the four models, indicating that neither out of roundness nor wall thinning had any appreciable influence on the magnitude of the maximum stresses.

The latter point is put in sharper perspective by also comparing the maximum stresses with NEE-theory predictions. Table 4.6 is a listing of

Table 4.5. Maximum normalized[a] experimental stresses[b] at elbow midsections for out-of-plane bending and for torsional moment loadings

Model	$\sigma_{\alpha o}$		$\sigma_{\alpha i}$		$\sigma_{\phi o}$		$\sigma_{\phi i}$	
	M_o	M_t	M_o	M_t	M_o	M_t	M_o	M_t
ME-1	2.75	2.75	1.4	1.4	2.49	2.65	-3.15	-3.12
ME-2	2.73	-2.7	1.3	-1.3	2.89	-2.9	-3.4	3.2
ME-3	2.6	-2.71	1.4	-1.37	2.60	-2.7	-3.0	3.25
ME-4	2.75	-2.95	1.5	-1.5	2.7	-2.91	-3.2	3.4

[a]Stresses are normalized to the loadings given in Table 3.2 so that the results appear as experimental stress indices.

[b]Values reported here were estimated by interpolation between gage sites; σ_α and σ_ϕ are longitudinal and circumferential stresses, respectively. Subscripts o and i indicate outside and inside surfaces, respectively.

Table 4.6. Out-of-plane and torsional moment stress indices[a] at elbow midsection

Model	NEE theory[b]	Maximum circumferential stress				Maximum principal stress			
		M_o	M_t	Average	Difference (%)	M_o	M_t	Average	Difference (%)
ME-1	3.32	3.15	3.12	3.135	-5.6	3.24	3.24	3.24	-2.4
ME-2	3.36	3.4	3.2	3.30	-1.8	3.42	3.38	3.40	+1.2
ME-3	3.46	3.0	3.25	3.125	-9.7	3.12	3.34	3.23	-6.6
ME-4	3.54	3.2	3.4	3.30	-6.8	3.28	3.50	3.39	-4.2

[a] Values reported here were estimated by interpolation between gage sites. See Appendix B for experimental data.

[b] NEE theory for M_o loading, ELBOW computer program for elbows with $\gamma = r/R = 3$ gives the approximate formula:

$$C_{2o} = 1.823\ \lambda^{-0.643} \cos\alpha;\ 0.01 \leq \lambda \leq 1.0;\ \alpha = 45^\circ.$$

the maximum circumferential and maximum principal stress indices for station 7 and the NEE-theory predictions for out-of-plane bending. Although the NEE-theory values do not include the effects of shear stresses, the comparisons indicate that these effects are on the order of only about 3% and therefore can be safely ignored in relation to the maximum circumferential stress. The usual assumption in NEE theory is that a torsional moment on the cross section of an elbow produces a uniform shear stress of the same magnitude as for a straight cylindrical shell. Examination of the data in Appendix B, however, shows that even though the shear stresses are small, the distribution is not uniform around the cross section. Further study, however, is needed before the NEE-theory assumption is altered.

The data in Table 4.6 show clearly that neither out of roundness nor wall thinning had much of an influence on the maximum stresses. The numbers indicate that out of roundness may have increased the maximum stress by about 3.8% (ME-2 vs ME-1) in close agreement with the predictions of Ref. 11 for elbows with 5% out of roundness (about 3.5% for b/c = 1.05). The wall thinning of ME-3 apparently decreased the maximum stress by about

4.1% (ME-3 vs ME-1). The effects of out of roundness and wall thinning together (ME-4) appear to be roughly additive as originally postulated.

End effects appear to have a significant influence on the stresses for both out-of-plane bending and torsional moment loading. Although the maximum stresses at the elbow midsection (Table 4.6) are only slightly less than predicted by NEE theory, the distribution along the length of the elbow is considerably different. Since $\bar{M}_t$ produces only shear stresses on the cross section, Eqs. (4.9) and (4.10) predict that the axial and circumferential stresses will be proportional to $\bar{M}_o$. Thus for out-of-plane bending, the stresses should be proportional to $M_o \cos \alpha$, with the maximum values occurring at the elbow-to-pipe junction (i.e., at station 10 where $\alpha = 0$); zero values would occur at the other end (station 4) where $\alpha = 90°$.

For torsional moment loading, the stresses should be proportional to $M_t \sin \alpha$, with the maximum values occurring at station 4 ($\alpha = 90°$). The data in Figs. 4.12–4.15, however, show that the stresses at station 4 are not zero for M_o loading and apparently are not a maximum for M_t loading. This phenomenon is referred to in Ref. 18 as a reverse end effect.

Figure 4.16 shows excellent agreement between the experimental data for the outside surface of ME-1 under M_o loading and the CURT-II analysis. As noted earlier the CURT-II analysis includes end effects but does not have the capability for considering out of roundness or wall thinning. The figure shows that both the axial and circumferential stresses are maximum somewhere between stations 8 and 9, with magnitudes of about 60 to 70% of the maximum values predicted by NEE theory for station 10.

4.4 Combined Moment and Pressure Loadings

In 1957, NEE-theory studies by Rodabaugh and George[4] on elbows and curved pipe with combined pressure and moment loadings showed that the *bending-moment stresses* are reduced by a nonlinear function of the internal pressure. Experimental data from in-plane moment tests on a large thin-walled long-radius welding elbow confirmed their theoretical conclusions. In 1972, Dodge and Moore[13] defined the moment-loading stress-index reduction factor $f(\lambda, \psi)$ based on Ref. 4 and results from an analytical

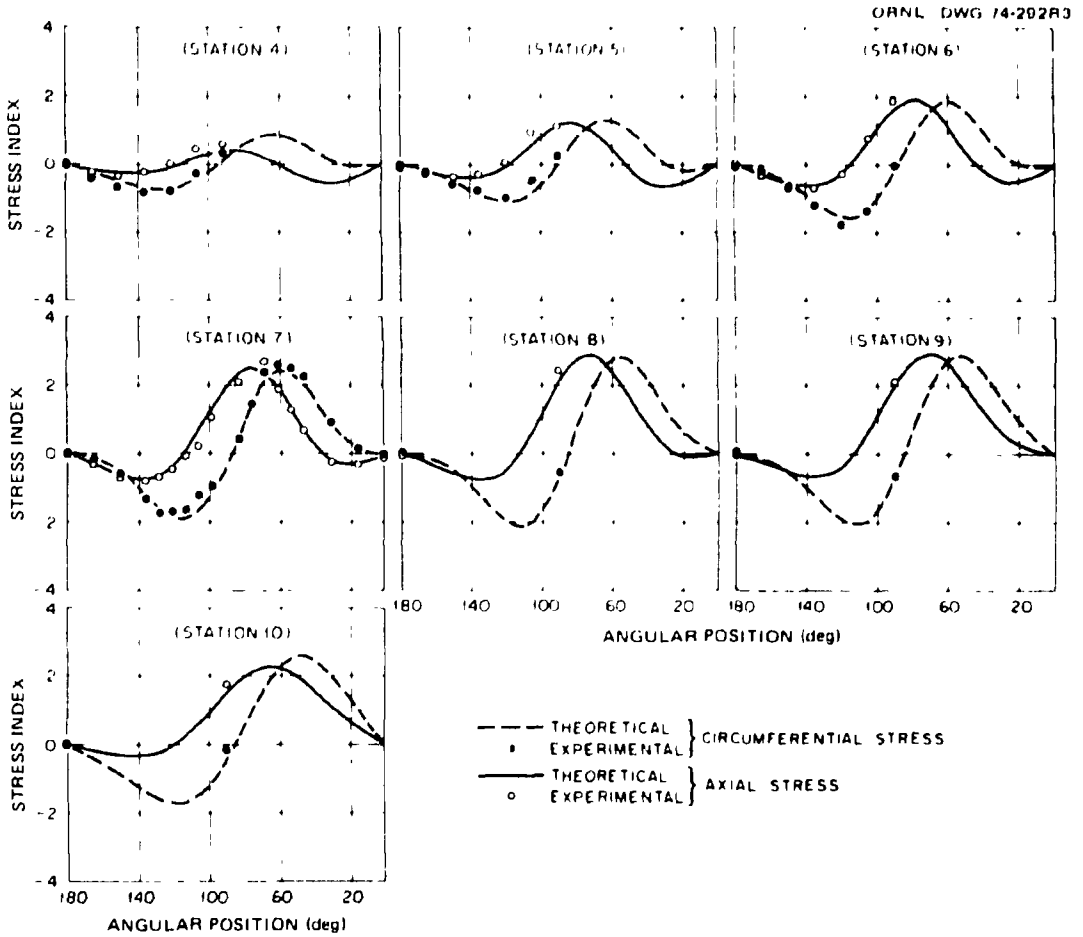

Fig. 4.16. Comparisons between CURT-II shell theory and experimental results for the outside surface of model ME-1 loaded with a simple out-of-plane moment M_o.

parameter study as:

$$f(\lambda, \psi) = [1 + \lambda^{-4/3} \exp(-\psi^{-1/4})]^{-1} , \tag{4.11}$$

where the bend characteristic λ and the nondimensional pressure parameter ψ are defined as:

$$\lambda = tR/(r^2 \sqrt{1 - \nu^2}) , \tag{4.12}$$

$$\psi = PR^2/Ert . \tag{4.13}$$

For the elbows in the current study, the numerical values of ψ/P range between 3.856×10^{-6} and 4.176×10^{-6} (see Table 2.1). Numerical

values of $f(\lambda, \psi)$, corresponding to the maximum pressures used in the combined loading tests, range between 0.841 and 0.928. Thus, NEE theory predicts a reduction in the moment-loading stress index due to internal pressure that ranges between 7.2 and 15.9%.

Table 4.7 gives a listing of the experimental moment-loading stress indices for both zero pressure and the maximum pressures. In all cases but one (ME-3 with M_t), the magnitude of the internal pressure influence was smaller than predicted. In several cases there appeared to be a slight increase in the stress index rather than a decrease, as shown in Fig. 4.17 for ME-1 with M_i.

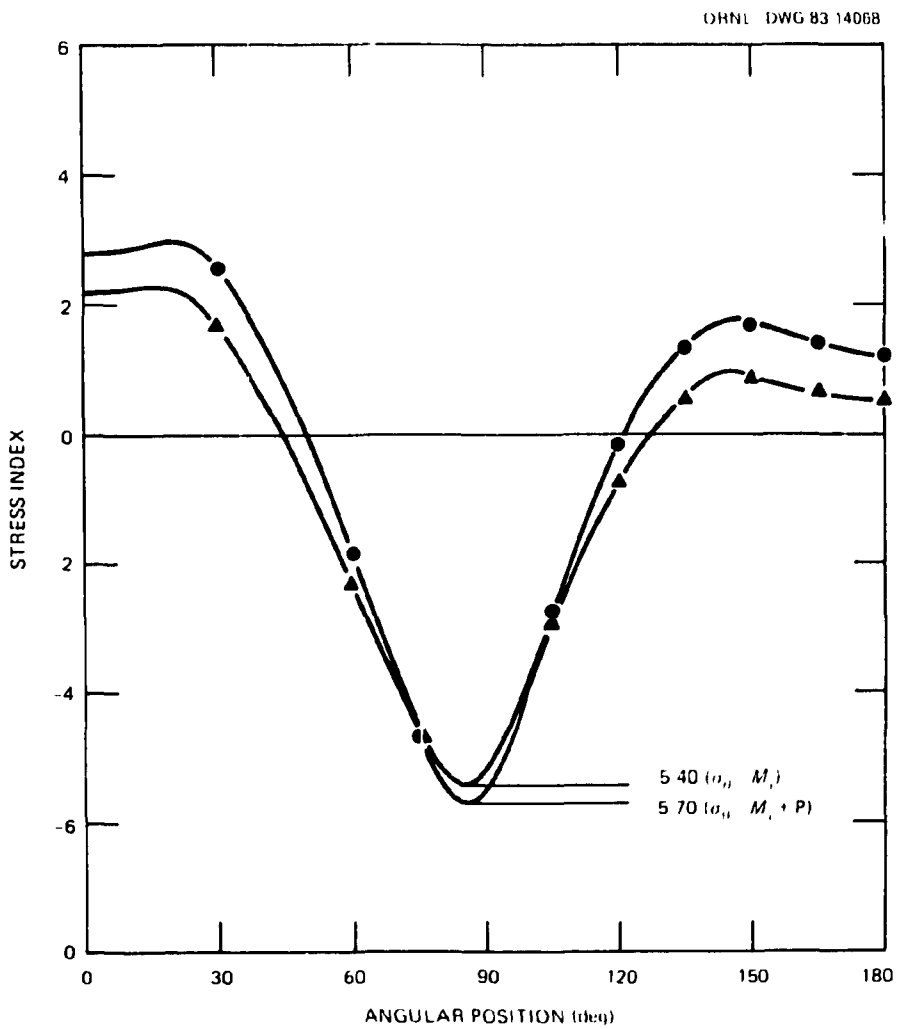

Fig. 4.17. Comparisons between circumferential stress distributions at station 7 for model ME-1 loaded with a simple in-plane moment M_i and with a combined moment-pressure (M_i + P) loading.

Table 4.7. Maximum principal stresses[a] at elbow midsection for moment loadings with and without internal pressure

Model	$f(\lambda, \psi)$	In-plane moment			Out-of-plane moment			Torsional moment		
		M_i	$M_i + Pb$	Difference (%)	M_o	$M_o + Pb$	Difference (%)	M_t	$M_t + Pb$	Difference (%)
ME-1	0.857	-5.40[c]	-5.70[c]	5.6	-3.24	-3.28	1.2	-3.24	-3.35	3.4
ME-2	0.928	-4.40	-4.50	2.3	-3.42	-3.38	1.2	3.38	3.10	8.3
ME-3	0.841	-4.60	-4.50	2.2	-3.12	-3.22	3.2	3.34	2.70	27.5
ME-4	0.915	-4.30	-4.00	0.7	-3.28	-3.23	1.5	3.50	3.20	8.6

[a]Stresses given here and in Appendix B are total stresses minus the stresses from internal pressure with zero moment load. Values are maximums interpolated between gage sites.

[b]Pressure loads were 1305 psi for ME-1 and ME-3 and 600 psi for ME-2 and ME-4.

[c]These values were difficult to estimate because of the loss of several strain gages in the vicinity of the maximum.

For ME-3 with a torsional moment M_t, the effect of combined pressure was greater than predicted – 27.5% vs 15.9%. For this case the pressure effect was actually somewhat greater than indicated by the numbers in Table 4.7. Figure 4.18 shows the maximum and minimum principal stress indices, $\bar{\sigma}_{max}$ and $\bar{\sigma}_{min}$, at the midsection of ME-3. Curves are shown for M_t acting alone and in combination with 1305 psi internal pressure. Both $\bar{\sigma}_{max}$ and $\bar{\sigma}_{min}$ are algebraically reduced by the pressure. In this case the

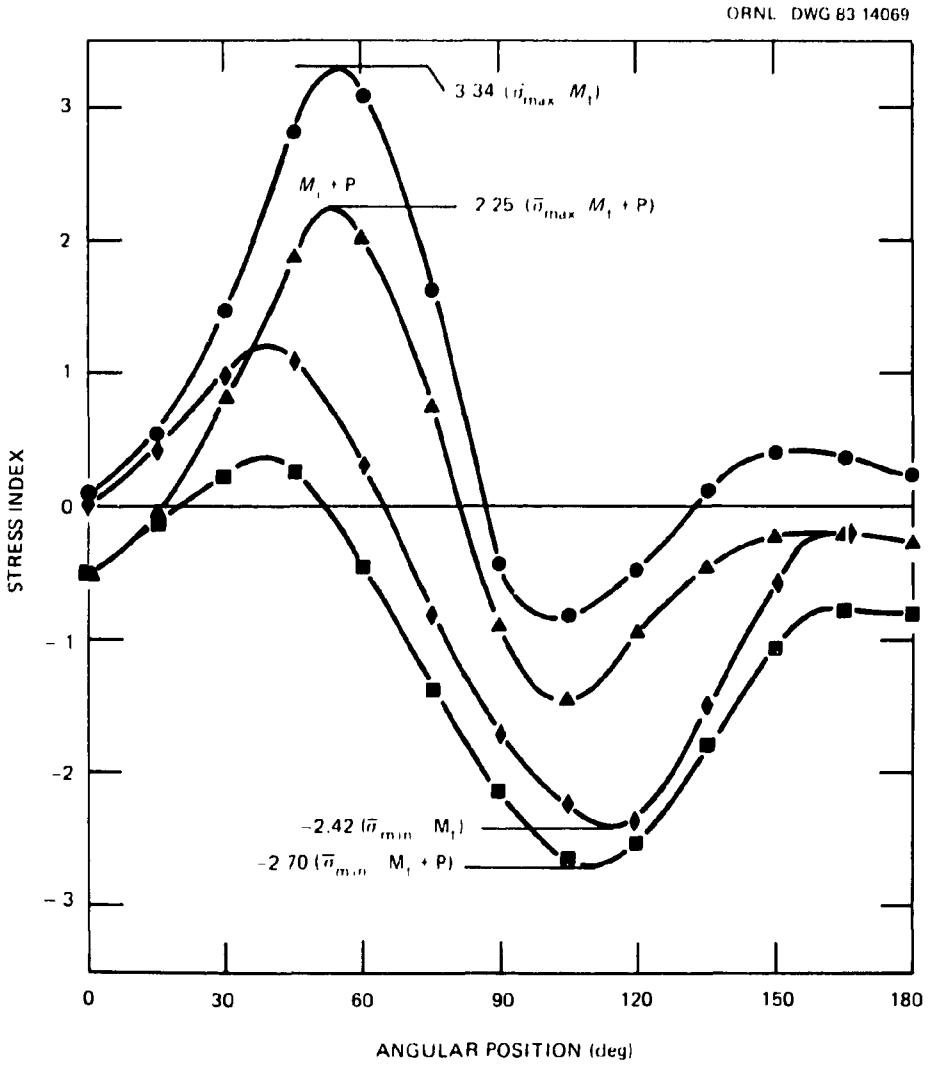

Fig. 4.18. Comparisons between principal stress distributions at station 7 for model ME-3 loaded with a simple torsional moment M_t and with a combined moment-pressure (M_t + P) loading.

algebraic reduction was sufficiently great to shift the location of the *absolute* maximum from $\bar{\sigma}_{max}$ at 52.5° to $\bar{\sigma}_{min}$ at 112.5°.

For this particular series of tests, NEE theory and the experimental data both indicate that the combined pressure-moment effect is not a significant factor for design purposes. It might also be noted that the influence of internal pressure on the moment-loading stress-index for elbows with attached straight pipe is more complicated than indicated by the relatively simple NEE theories.

5. SUMMARY AND CONCLUSIONS

The experimental study described in this report was undertaken primarily to measure the effects of out of roundness and wall-thickness variations on the maximum stresses in piping elbows under internal pressure and bending-moment loads. Two other objectives were to study the effects of end restraint from the attached piping (end effects) and the effects of the internal pressure and bending moment interactions.

To accomplish these objectives, four 10-in. NPS, 90°, long-radius, schedule 40, carbon-steel piping elbows were specially manufactured and tested. Dimensional characteristics of the four elbows were as follows:

Model	Cross-section shape	Wall thickness
ME-1	Circular	Uniform
ME-2	Out of round (elliptical)	Uniform
ME-3	Circular	Variable (eccentric bore)
ME-4	Out of round (elliptical)	Variable (eccentric bore)

Complete wall-thickness and outside-diameter profiles were made for each elbow prior to fabricating and instrumenting the test models. Each test model consisted of an elbow and two short pieces of schedule 40 carbon-steel pipe (round or partially flattened) welded to the two ends of the elbow, along with end closures and suitable loading fixtures. Each model was instrumented with approximately 90 three-gage strain rosettes, distributed on both the inside and outside surfaces at the center of the elbow and on the outside surface along the length of the model. Strain gage and load cell data were obtained with a 1000 channel computer-controlled data acquisition system and recorded on magnetic tape.

Each of the four models was tested with internal-pressure; with in-plane, out-of-plane, and torsional moment loads acting separately; and with combined pressure-moment loads. At the end of each loading sequence, all the load-strain data were analyzed for linearity and repeatability, and best fit load-strain relationships were established for each gage using an ORNL strain gage diagnostic computer program. Normalized stresses

(experimental stress indices) were then calculated, plotted, and compared with various theoretical solutions.

Results from the experimental data show that theoretical stress analysis solutions based on NEE theory capture the major characteristics of the stress distributions for elbows loaded with either internal pressure or applied moment loads. Of the four items addressed in this study, end effects had the most influence on the stresses, followed in order by out of roundness, variations in wall thickness, and pressure-moment interactions. Of these, the only significant *increase* in maximum stresses above those predicted by NEE theory was produced by out of roundness for internal pressure loadings. The influence of each of the four items on maximum stresses is discussed below.

5.1 End Effects

The experimental data show that end effects caused a general reduction in the stresses predicted by NEE theory, with the major reduction being at the elbow-to-pipe junctions and a much smaller reduction at the center of the bend. For internal pressure loading, end effects were most notable for the out-of-round models ME-2 and ME-4, where shell-bending stresses were present. The membrane stresses in all four models agreed fairly well with the NEE membrane-stress theory of Lorenz, with the circumferential membrane stresses being somewhat less than predicted.

For in-plane moment loadings, end effects reduced the maximum stresses by about 4% at the elbow midsections and by about 60-65% at the elbow-to-pipe junctions.

For out-of-plane and torsional moment loadings the situation is somewhat more complicated. For these loadings, NEE theory predicts that the maximum normal stresses in a 90° elbow will occur at one end and that only shear stresses will occur at the other end. The test data show, however, that end effects cause a shift in location of the maximum stress to a point about midway between the midsection and end of the elbow and a reduction of about 30-40% of the NEE-theory prediction. At the other end, where NEE theory predicts only shear stresses, end effects produce normal stresses as well as shear stresses. At the midsection of the elbow, end

effects reduced the maximum circumferential stress predicted by NEE theory by about 6% but only reduced the maximum principal stress by about 2.5% because of the additional shear stresses on the cross section.

End effects were accurately predicted by both the finite-element computer code EPACA and the thin-shell-theory program CURT-II for in-plane and out-of-plane moment loadings on ME-1. Although none of the other models were analyzed with these methods, it should be feasible to obtain good results with the finite-element program if suitable mesh layouts are developed. Major changes, however, would be required in the thin-shell-theory program to accommodate the geometric variations.

5.2 Out of Roundness

In this study, the effects of out of roundness were deduced by comparing experimental data from the two out-of-round models ME-2 and ME-4 with experimental data from the baseline model ME-1 and with analytical NEE-theory results. For internal pressure loads, these comparisons showed that out of roundness causes a significant increase in the maximum stresses by introducing shell-bending stresses into the body of the elbow that are only partially mitigated by end effects. Reasonable agreements were obtained between the maximum experimental circumferential-bending stress and Rodabaugh's out-of-round pipe theory.

Rodabaugh's theory is the basis for the ASME Code stress index K_1 for out-of-round elbows. Consequently, our experimental data tends to support the validity of the Code index. Because of the limitations inherent in Rodabaugh's theory, however, additional theoretical development work needs to be done to describe the longitudinal stresses as well as the circumferential stresses, and to include the bend radius as a parameter.

For the three moment loads, the effects of out of roundness were deduced by comparing the experimental data with NEE-theory results (ELBOW) and with Findlay and Spence's elliptical elbow theory. The only effect that may be attributable to out of roundness was a reduction in the circumferential stresses at the midsection of the elbows (ME-2 and ME-4) of about 20% for in-plane moment loadings. It is postulated, however, that if the out of roundness had been perpendicular to the plane of the bend,

the experimental data might have shown an increase in the circumferential stresses. The NEE theory of Findlay and Spence[11] predicts less than 2% reduction in the maximum circumferential stresses. The apparent anomaly suggests that additional experimental and/or theoretical work needs to be done before definite conclusions are reached. Essentially no reduction was observed in the longitudinal stresses for in-plane moment or in either the circumferential or longitudinal stresses for out-of-plane and torsional moments.

5.3 Variable Wall Thickness

As far as we were able to determine from the four experimental models studied, a variable wall thickness has no *direct* influence on the stresses from either internal-pressure or applied-moment loadings. There did appear to be third-order effects when wall-thickness variations were combined with out of roundness, but these may also be attributed to scatter in the experimental data. As with out of roundness, however, there was one anomalous case (ME-3 with M_i) where the maximum circumferential stresses were reduced by about 20%. We do not have any analytical models with which to compare the experimental data.

5.4 Combined Pressure-Moment Loadings

Although NEE theory predicts a small general reduction in the moment-loading stress indices as a function of increasing internal pressure, the experimental data failed to support that conclusion. Of the 12 elbow-loading cases studied, only 3 showed a reduction in the absolute value of the principal stresses as large as predicted by NEE theory. Five cases actually showed a small increase. Even though the loss of several critical strain gages made comparisons difficult, the study clearly shows that combined pressure-moment effects are more complicated than indicated by the relatively simple NEE theories. Further studies of combined pressure-moment effects should be done in conjunction with improved solutions that include the effects of end conditions.

5.5 Conclusions

The experimental stress analysis study of 90° elbows presented in this report supports the following conclusions:

1. Analytical solutions based on NEE theories capture the major characteristics of the stress distributions for elbows loaded with either internal-pressure or applied-moment loads.

2. End effects cause a general reduction in the magnitude of the stresses predicted by NEE theory, with the major reduction being at the elbow-to-pipe junctions and much smaller reduction at the center of the bend.

3. End effects cause a larger reduction in the maximum NEE-theory stresses for 90° elbows loaded with out-of-plane or torsional moments than for 90° elbows loaded with in-plane moments or internal pressure.

4. Out of roundness causes a significant increase in the maximum NEE-theory stresses for elbows loaded with internal pressure.

5. Under certain conditions, out of roundness may cause a significant increase in the NEE-theory stresses for in-plane moment loads, although additional experimental and analytical work is needed for confirmation.

6. Wall-thickness variations on the order of $\pm 25\%$ of nominal appear to have no direct influence on the stresses for either internal-pressure or applied-moment loads. Theoretical studies, however, are needed to confirm this conclusion.

7. Combined internal-pressure and moment loadings on 90° elbows with attached pipes produce a more complicated stress pattern than predicted by NEE theories. Further analytical studies that also include the effects of end conditions are needed to better understand the phenomena.

8. The experimental data presented in this report should be a valuable resource for further study directed toward developing improved theoretical solutions and/or improved design rules.

REFERENCES

1. ANSI Standard B16.9-78, *Factory-Made Wrought Steel Butt Welding Fittings*, American Society of Mechanical Engineers, New York, 1978.

2. Manufacturer's Standardization Society, *Factory-Made Butt-Welding Fittings for Class 1 Nuclear Piping Applications*, MSS-SP87, 1977.

3. *ASME Boiler and Pressure Vessel Code, Nuclear Power Plant Components*, Sect. III, Div. 1, American Society of Mechanical Engineers, New York, 1980.

4. E. C. Rodabaugh and H. H. George, "Effect of Internal Pressure on Flexibility and Stress-Intensification Factors of Curved Pipe or Welding Elbows," *Trans. ASME* 79, 939–48 (1957).

5. W. G. Dodge and J. E. Smith, *A Diagnostic Procedure for the Evaluation of Strain Data from a Linear Elastic Test*, ORNL/TM-3415, Union Carbide Corp. Nuclear Div., Oak Ridge Natl. Lab., November 1972.

6. C. C. Perry and H. R. Lissner, *The Strain Gage Primer*, McGraw-Hill, New York, 1955.

7. H. Lorenz, "Theörie der Rohrenfedermanometer," *VDI Z.* 54, 1865–67 (1910).

8. Z. Zudans et al., *Theory and Users Manual for EPACA*, F-C3038, Franklin Institute, June 30, 1972.

9. R. C. Gwaltney, *CURT-II – A Computer Program for Analyzing Curved Tubes or Elbows and Attached Pipe with Symmetric and Unsymmetric Loadings*, ORNL/TM-4646, Union Carbide Corp. Nuclear Div., Oak Ridge Natl. Lab., November 1974.

10. A. Kalnins, "Stress Analysis of Curved Tubes – A User's Manual," Lehigh University, Bethlehem, Penn., May 31, 1968.

11. G. E. Findlay and J. Spence, *Bending of Pipe Bends with Elliptic Cross Sections*, Welding Research Council Bulletin 164, August 1971.

12. W. G. Dodge and S. E. Moore, *ELBOW: A Fortran Program for the Calculation of Stresses, Stress Indices, and Flexibility Factors for Elbows and Curved Pipe*, ORNL/TM-4098, Union Carbide Corp. Nuclear Div., Oak Ridge Natl. Lab., April 1973.

13. W. G. Dodge and S. E. Moore, *Stress Indices and Flexibility Factors for Moment Loadings on Elbows and Curved Pipe*, Welding Research Council Bulletin 179, December 1972.

14. R. A. Clark, T. I. Gilroy, and E. Reissner, "Stresses and Deformations of Toroidal Shells of Elliptical Cross Section," *J. Appl. Mech.* 19, 37–48 (1952).

15. E. C. Rodabaugh, *Stresses in Out-of-Round Pipe Due to Internal Pressure*, ORNL/TM-3244, Union Carbide Corp. Nuclear Div., Oak Ridge Natl. Lab., January 1971.

16. B. P. Haigh, "An Estimate of the Bending Stresses Induced by Pressure in a Tube that is not Initially Quite Circular," *Proc. Inst. Mech. Engrs.* 133, 96–98 (1936).

17. Th. von Karman, "Über die Formänderung dünnwandieger Rohre, insbersondere federnder Ausgliechrohre," *VDI Z.* 55, 1889–95 (1911).

18. E. C. Rodabaugh and S. E. Moore, "End Effects on Elbows Subjected to Moment Loadings," *Advances in Design and Analysis Methodology for Pressure Vessels and Piping*, B. C. Wei and C. E. Pugh (Eds.), PVP Vol. 56, 99–123, American Society of Mechanical Engineers, 1982.

Internal Distribution

1. S. E. Bolt
2. J. M. Corum
3. W. G. Dodge
4. D. S. Griffith
5-9. S. E. Moore
10. H. E. Trammell
11. G. T. Yahr
12. ORNL Patent Office
13. Central Research Library
14. Document Reference Section
15-16. Laboratory Records Department
17. Laboratory Records, ORNL RC

External Distribution

18-22. Naval Sea Systems Command, Washington, DC 20362

SEA 05R	1 copy
SEA 05R32 (DeCorpo)	1 copy
SEA 56D2 (Kemezis)	1 copy
SEA 56Y33	2 copies

23-37. David Taylor Naval Ship R&D Center, Annapolis Laboratory, Annapolis, MD 21402

Code 27	1 copy
Code 274	1 copy
Code 2740	1 copy
Code 2744	1 copy
Code 2744 (Kaldor)	10 copies
Code 2744 (Neilson)	1 copy

38. Office of Assistant Manager for Energy Research and Development, Department of Energy, Oak Ridge Operations Office, Oak Ridge, TN 37830
39-40. Technical Information Center, DOE, Oak Ridge, TN 37830